Chapter 8
Cracking Risk and Regulations

Agnieszka Knoppik, Jean-Michel Torrenti, Shingo Asamoto, Eduardus Koenders, Dirk Schlicke and Luis Ebensperger

Abstract This chapter is focused on the cracking risk at early ages. After general considerations about cracking, the cracking risk prediction is discussed. Two main ways to assess this risk are considered: through an evaluation of the tensile stresses and through an evaluation of the strains. Finally, the evaluation of crack opening at early ages and the reinforcement design in regulations are presented.

8.1 Introduction—Significance of Cracking

Cracking is a normal phenomenon in reinforced concrete structures. Indeed, to obtain a good use of the reinforcement (i.e. a high stress in the reinforcement), cracking should occur. But of course the crack opening should be limited (see Sect. 8.1.2).

To evaluate the crack opening (and the crack spacing), three levels of model could be used:

- **Level I**: In the reinforced concrete codes, safety factors affecting the materials and the loadings are considered. Assuming simple behaviour (generally a constant

A. Knoppik (✉)
Silesian University of Technology, Gliwice, Poland
e-mail: agnieszka.jedrzejewska@polsl.pl

J.-M. Torrenti
IFSTTAR, University Paris-Est, Champs-Sur-Marne, France

S. Asamoto
Saitama University, Saitama, Japan

E. Koenders
Technische Universität Darmstadt, Darmstadt, Germany

D. Schlicke
Graz University of Technology, Graz, Austria

L. Ebensperger
Construtechnik Ltda., Santiago, Chile

E. M. R. Fairbairn and M. Azenha (eds.), *Thermal Cracking of Massive Concrete Structures*, RILEM State-of-the-Art Reports 27,
https://doi.org/10.1007/978-3-319-76617-1_8

bond stress), the crack spacing, the stresses in the reinforcement and finally the crack opening could be calculated—see Sect. 8.2.4.

- **Level II**: The first-order second-moment method (FOSM) (Koenders et al. 2007) is a probabilistic approach for early-age cracking. It considers the probability of failure P_f as the probability of the tensile stress exceeding the tensile strength. This approach is presented in Sect. 8.3.
- **Level III**: A Monte Carlo approach can also be used. With this calculation procedure, all probability density functions of all strength and load variables are considered (Koenders et al. 2007)—see Sect. 8.3.

8.1.1 General Considerations About Crack Width

In the recent Model Code 2010 (CEB-FIP *fib* 2012), it is indicated that "*the phenomena of cracking are of highly probabilistic nature. Therefore, the comparison of calculated crack widths with nominal crack widths limits may only serve as an approximate means to satisfy the design criteria. High accuracy may not be expected*". Figure 8.1 shows an example of the distribution of maximal crack openings (ECP 2008).

The crack width w_k estimated by means of the Eurocode 2 (EN 1992-1-1 2004) corresponds indeed to a conventional crack width (or a design crack width), in a steady state.[1] In Eurocode 2, the index k means that it is a characteristic value.[2] The fractile is not defined in the text (like, for instance, it is for the compressive strength). In the 1978 version of the Model Code, a relation between the characteristic value and the mean value was proposed: $w_k = 1.7w_m$. This relation is coming from results of tests performed by Beeby (1972) and was used to elaborate the relations used in order to estimate the crack width (ECP 2008). Actually, the coefficient 1.7 is included in the coefficients that are used to estimate the maximum crack spacing $s_{r,\max}$ of Eurocode 2 and Model Code 2010.

Also, it should be noted that the crack width w_k corresponds to an opening measured at the concrete surface (this is not indicated in Eurocode 2 but it is in Model Code 2010; also the comparison between the proposed equations and tests is clearly made using surface measurements ECP 2008). And experimental results show that the larger the concrete cover the larger the crack width at concrete surface (cf. Figs. 8.2 and 8.3). This effect is taken into account in Eurocode 2 and Model Code 2010 in the estimation of the maximum crack spacing (and consequently in the crack width).

[1]The steady state corresponds to the moment where all the possible cracks are created. An increase of the loading will induct a larger crack opening. Before this steady state, the number and the spacing between cracks could be very different. Especially under imposed strains, the steady state is generally not obtained.

[2]In the MC2010, the crack width is clearly a design value and noted w_d

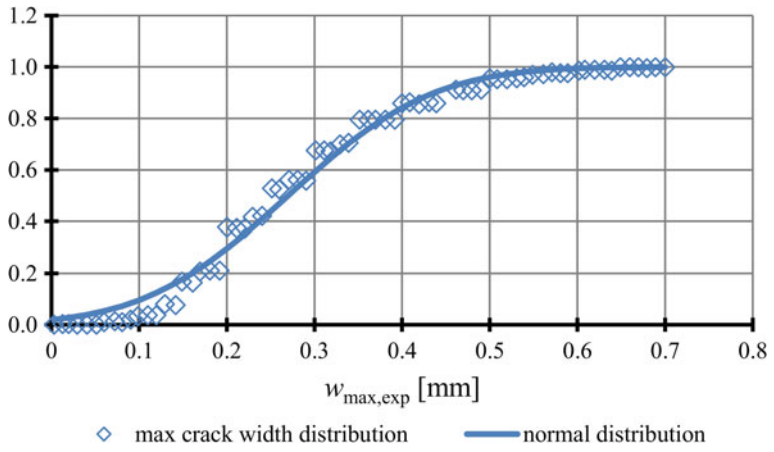

Fig. 8.1 Maximum experimental crack width distribution; after (ECP 2008)

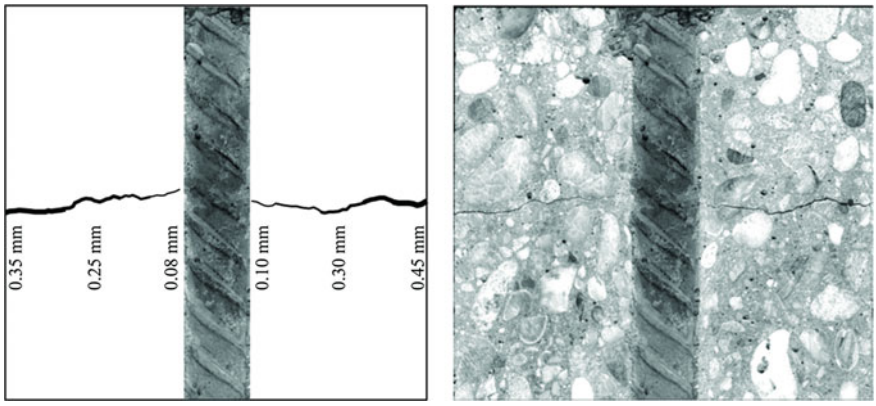

Fig. 8.2 Variation of crack width for specimen with concentric steel reinforcement (concrete cover of 50 mm); after (Borosnyoi and Snobli 2010). Cracking is obtained by means of direct tension. A resin is injected within cracks of the widths of 0.05–0.50 mm under sustained loading. The load was released only after the resin was allowed to set. Then, the samples were sawn. So, the crack width corresponds to a service state

8.1.2 Crack Width and Performance

For classical reinforced or prestressed structures, leakage is irrelevant or a limited leakage is accepted, and the control of cracking mainly aims at limiting the stress variations in the reinforcement and ensuring durability, aspect preservation, and

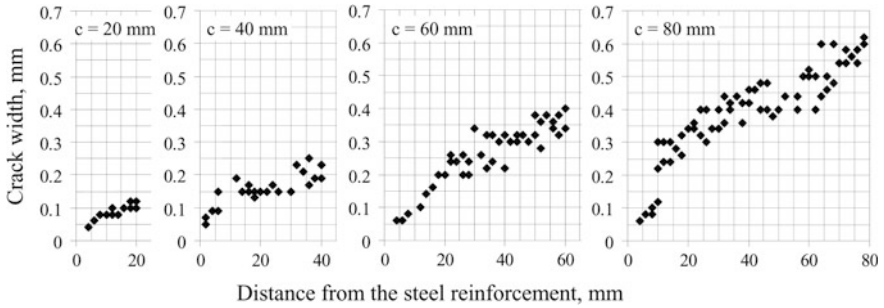

Fig. 8.3 Variation of crack width for specimens with eccentric steel reinforcement (concrete covers of 20, 40, 60, 80 mm); after (Borosnyoi and Snobli 2010)

continuity in the structural behaviour. In these structures, the crack opening is limited for durability reasons. Indeed, the cracking affects the transport properties of aggressive agents such as CO_2 and chloride ions. The admissible crack opening depends on environmental exposure according to the location and type of the structure. For instance, for Eurocode 2, if corrosion due to carbonation is the main risk, the crack opening should be limited to 0.3 mm. This limitation of the crack width ensures that the structural performance is not affected. Table 8.1 gives an example for the maximum allowable crack widths for reinforced concrete under service loads (ACI 224 2001).

In case of structures where tightness is an explicit operational requirement, the crack width should be lower, especially if the cracks are due to restrained shrinkage. This could be explained by the fact that—in the first approximation—permeability and diffusivity are proportional to the power of 3 of the crack opening and to the crack opening, respectively. In this case, the opening of possible cracks produced at early age due to restrained thermal or desiccation shrinkage, mechanical loadings during the execution phases, as well as the crack opening due to further service loading(s) associated to the tightness verification scenarios shall be considered and compared to the maximum design crack opening (Barre et al. 2016).

Note that due to possible self-healing, the crack width could be reduced with time (in a natural manner or with the use of permeability-reducing admixtures).

Table 8.1 Maximum allowable crack width in (ACI 224 2001)

Exposure condition	Crack width [mm]
Dry air or protective membrane	0.41
Humidity, moist air, soil	0.30
De-icing chemicals	0.18
Seawater and seawater spray, wetting and drying	0.15
Water-retaining structures	0.10

Fig. 8.4 Water treatment plant showing cracking due to the restrained shrinkage at early age and some self-healed cracks (photograph: A. Darquennes)

That is why the recent CEB-FIP *fib* Model Code 2010 (CEB-FIP *fib* 2012) indicates that "*with regard to crack width limitation for fluid-tightness […] if leakage should be limited to a small amount and some surface staining is acceptable* w_{lim} *= 0.20 mm may be used as a limit for self-healing cracks. Otherwise 0.1 mm may be more appropriate.*" Model Code 2010 specifies that "*whether self-healing of cracks can occur depends on the chemical composition of the fluid, type of cement, water pressure, time after subjecting to water pressure,* etc." Figure 8.4 gives an example of a water tank where some self-healing has closed some of the cracks.

8.2 Crack Risk Prediction

8.2.1 Role of Boundary Conditions

Concrete elements are subjected to early-age volume changes due to temperature and moisture variations which characterise the process of concrete hardening. These volume changes induce stresses in concrete elements. In massive concrete elements, such as foundation slabs or blocks, the stresses are induced mainly by significant temperature gradients developing between the interior and the surface of the element (the so-called self-induced stresses, self-balanced stresses or *Eigenstresses*). In externally restrained elements, such as walls, thermal–shrinkage stresses result from a coupled action of self-induced and restraint stresses. The restraint in these

elements is exerted by the bond between the new concrete of the element and the older concrete of the foundation or previous lift.

Stresses in the internally restrained elements result from volume changes due to temperature and moisture gradients. In such case, an internal restraint is induced and it is caused by a temperature and moisture difference within the section. In such elements, random crack maps on surfaces can be usually observed. Stresses in the externally restrained elements are caused by bond forces generated in the joint between the element and the restraining body. The main causes of the bond force generation are unbalanced thermal–shrinkage strains in the element and the restraining body if the two are executed separately one after another. In a typical externally restrained element, restraint stresses play a predominant role because volumetric strains caused by the temperature and humidity gradients are relatively small in comparison to the linear strains caused by the contraction of the element along the line of the restraint joint. Nevertheless, it must be remembered that with the increasing massiveness the share of the self-induced stresses increases. Surface tensile stresses occurring in thick walls (thermal gradients) and formed by early formwork removal (both thermal and moisture gradients) may lead to surface cracking which can further develop into through cracking in superposition with external restraint.

A typical pattern of cracking due to the edge restraint is shown in Fig. 8.5a. Without a restraint, the section would contract along the line of the base, and so with the restraint a horizontal force develops along the construction joint. The occurring cracks are vertical in the central part of the wall and splay towards the ends of the element where a vertical tensile force is required to balance the tendency of the horizontal force to warp the wall. A horizontal crack may occur at the construction joint at the ends of the walls due to this warping restraint. Figure 8.5b presents the cracking of the wall with end restraint. The external restraint might be a combination of a base and a side restraint (Fig. 8.5c, d). Usually, the first crack occurs at the construction joint as the strength of the bond between the new and mature concrete is less than the tensile strength of the element. Such a crack is therefore less likely to be fully developed. If the overall contraction of the wall can be satisfied by fully developed cracks at one or both construction joints, then the intermediate cracks shown in Fig. 8.5c, d may not occur.

In a typical base-restrained element, the occurring cracks have vertical alignment and may reach a significant height. The greatest height of the crack is observed in the middle of the element and it declines towards the side edges or towards the expansion joints. The maximum width of the crack occurs at some level above the joint (Flaga and Furtak 2009; Nilsson 2000). The extent and size of cracking depend on the amount and distribution of the applied reinforcement: When sufficient reinforcement is provided, the widths of the primary cracks are controlled but secondary cracks may be induced (ACI 207.1 2005; Mihashi and Leite 2004; RILEM TC 119-TCE 1997; RILEM TC 181-EAS 2002). Design of reinforcement and its influence on cracking pattern is further discussed in Sect. 8.4.

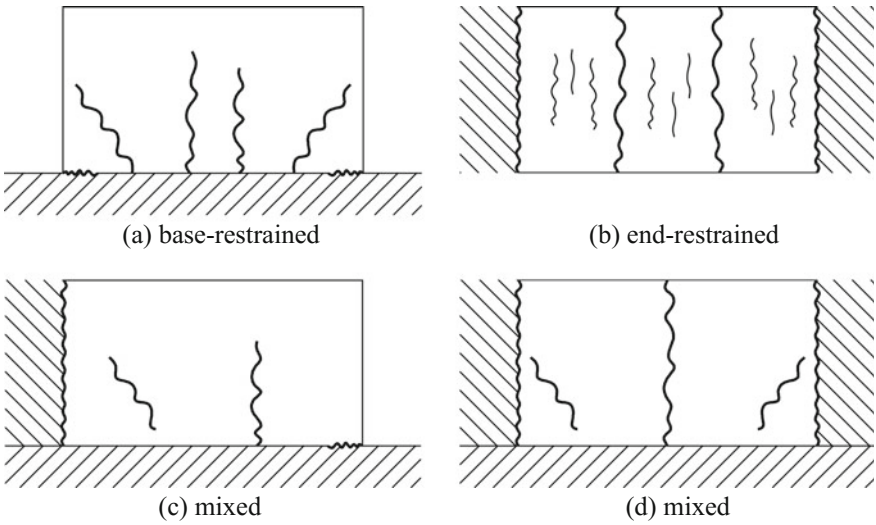

Fig. 8.5 Cracking pattern in restrained elements after (Knoppik-Wróbel 2015)

8.2.2 *Stress Approach Versus Strain Approach*

There are two basic approaches in crack risk prediction. The stress approach postulates that the crack is formed when the stress in a given point determined under the assumption of uncracked sections exceeds the actual tensile strength in that point. The maximum tensile stress σ_{ct} is compared with tensile strength f_t. If $\sigma_{ct} > f_t$, a crack is formed.

In the strain approach, the restrained strain is determined taking into account the effect of restraint, creep and sustained loading:

$$\varepsilon(x, y, z, t) = R(x, y, z) \cdot \varepsilon_{\text{free}}(x, y, z, t) \cdot \varphi \tag{8.1}$$

where

$\varepsilon_{\text{free}}(x, y, z, t)$ free strain in a given location (x, y, z) at time t,
$R(x, y, z)$ restraint coefficient in a given location (x, y, z),
φ creep coefficient (≤ 1).

This strain is then compared with the strain capacity, which relates tensile strength $f_t(t)$ and Young's modulus $E_c(t)$:

$$\varepsilon_{ctu}(t) = \frac{f_t(t)}{E_c(t)} \tag{8.2}$$

The crack is formed when $\varepsilon > \varepsilon_{ctu}$.

Comparing the two approaches, it can be concluded that conceptually stress and strain approaches can be used interchangeably. The approaches differ in detailed methods for determination of the subsequent components, i.e. strains, restraint coefficients and mechanical properties. Section 8.2.3 discusses the methods based on the stress approach while Sect. 8.2.4 discusses the strain approach.

8.2.3 Stress Approach and Cracking Index

8.2.3.1 Compensation Plane Method (JSCE 2011)

The compensation plane method (CPM) was developed by the Technical Committee of the Japan Concrete Institute in 1985 (JCI 1985) and is recommended in the JSCE Guideline no. 15. The method is based on the fact that the early-age stresses in hardening concrete elements result from a coupled action of internal and external restraints of strain. The total strain results from thermal strain (usually a gradient is considered) and shrinkage strain (usually limited to autogenous shrinkage which is assumed uniform). The method had been used mainly for slab and wall structures as the most practical method in Japan. Recently, the thermal cracking for various massive structures has been assessed based on 3D finite element method proposed by JCI guideline (JCI 2008) and AIJ Guideline (AIJ 2008)—please refer to Sect. 8.2.3.2.

The stress exerted due to the internal restraint is caused by a differential strain in the cross section resulting from the temperature (and moisture) gradients. The increment of stress $\Delta\sigma_{\text{int\_}i}$ between ages of t_{i-1} and t_i due to the internal restraint can be determined from the difference between the strain value at a point of the compensation line, $\varepsilon_{\text{comp}}$, and the thermal–shrinkage strain distribution curve, ε_0, by the equation (see Fig. 8.6):

$$\Delta\sigma_{\text{int\_}i}(x,z) = E_c(t_i) \cdot \left(\varepsilon_0(x,z) - \varepsilon_{\text{comp}}\right) \tag{8.3}$$

$$\varepsilon_0(x,z) = CTE \cdot \Delta T_i(x,z) \tag{8.4}$$

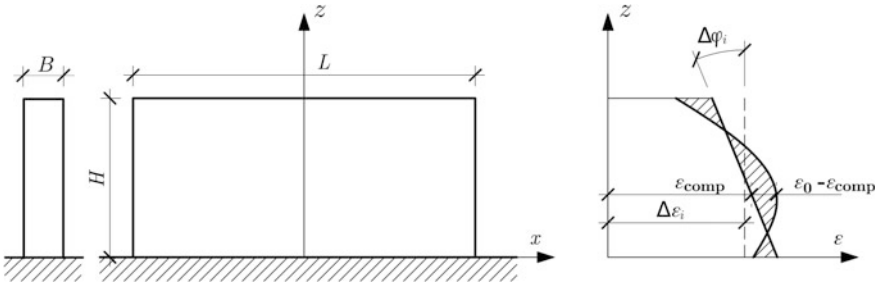

Fig. 8.6 Determination of stresses in a wall-on-slab structure caused by internal restraint according to compensation plane method according to (JSCE 2011)

where

$E_c(t_i)$ Young's modulus of concrete at the age of t_i,
CTE coefficient of thermal expansion of concrete,
$\Delta T_i(x, z)$ temperature difference between ages of t_{i-1} and t_i at point (x, z).

To determine the location of the compensation plane (zero-stress plane), equilibrium of stress block must be determined. For section stability, the sum of tensile stress induced by the temperature or moisture gradient in a cross section should be balanced by an equal compressive force. This approach allows obtaining the increment of the free axial strain $\Delta\varepsilon_i$, and the increment of curvature $\Delta\phi_i$.

$$\Delta\varepsilon_i = \frac{1}{A}\int \varepsilon_0(x,z)\mathrm{d}A \tag{8.5}$$

$$\Delta\phi_i = \frac{\int (\varepsilon_0(x,z) - \Delta\varepsilon_i)(z - z_{\mathrm{cen}})\mathrm{d}A}{I} \tag{8.6}$$

$$\varepsilon_{\mathrm{comp}} = \Delta\varepsilon_i + \Delta\phi_i(z - z_{\mathrm{cen}}) \tag{8.7}$$

where

A area of concrete cross section,
z_{cen} centre of gravity of concrete cross section,
I moment of inertia of area of concrete cross section.

The internal forces due to the external restraint are generated in the element trying to return the plane after deformation to the original restrained position—axial force ΔN_R and bending moment ΔM_R from the age of t_{i-1} to the age of t_i. The increment of stress due to the external restraint $\Delta\sigma_{\mathrm{ext\_}i}$ is determined by the coupled action of the axial force and bending moment, as presented in Fig. 8.7, according to the equation:

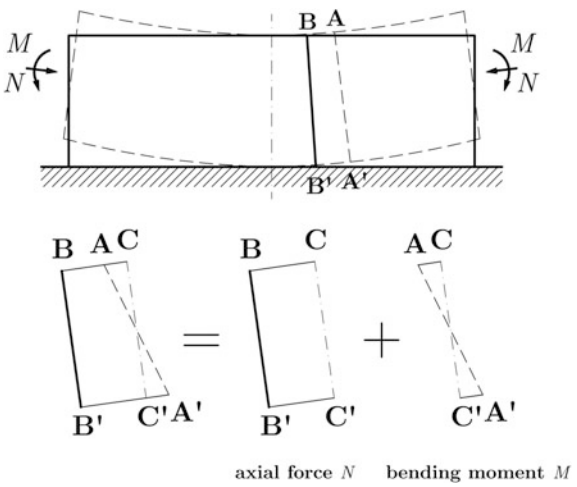

Fig. 8.7 Determination of stresses in a concrete element caused by external restraint according to compensation plane method according to (JSCE 2011)

$$\Delta\sigma_{\text{ext\_}i}(x,z) = \frac{\Delta N_R}{A} + \frac{\Delta M_R}{I}(z - z_{\text{cen}}) \tag{8.8}$$

The internal forces can be defined as follows:

$$\begin{aligned} \Delta N_R &= R_N \cdot E_c(t_i) \cdot A \cdot \Delta\varepsilon_i \\ \Delta M_R &= R_M \cdot E_c(t_i) \cdot I \cdot \Delta\phi_i \end{aligned} \tag{8.9}$$

where

R_N external restraint coefficient for the degree of axial deformation restraint,
R_M external restraint coefficient for the degree of flexural deformation restraint.

The external restraint coefficients are introduced to represent the degree of restraint of the element by the restraining body. Equation 8.8 gets a form:

$$\Delta\sigma_{\text{ext\_}i}(x,z) = R_N \cdot E_c(t_i) \cdot \Delta\varepsilon_i + R_M \cdot E_c(t_i) \cdot \Delta\phi_i \cdot (z - z_{\text{cen}}) \tag{8.10}$$

and the total thermal–shrinkage stress at any position (x, z) can be calculated as:

$$\sigma_{\text{tot}}(x,z) = \sum\nolimits_i \{\Delta\sigma_{\text{int\_}i}(x,z) + \Delta\sigma_{\text{ext\_}i}(x,z)\} \tag{8.11}$$

The values of the restraint coefficients vary within the element according to the degree of restraint. They depend on the difference in stiffness between the restraining body and the early-age concrete element as well as the ratio of the length to the height of the element (L/H). For that purpose the functions of the restraining factors need to be defined. JSCE Guideline no. 15 (JSCE 2011) proposes diagrams of restraining factors, determined with 3D numerical calculations.

Methods based on similar approach can be found in other standards worldwide. Eurocode 2 in Part 3 (EN 1992-3 2008) proposes to determine stress distribution due to translational and rotational restraint of the element based on the known imposed strain from the equation:

$$\sigma(z) = E_c(t_i) \cdot (\varepsilon_i(z) - \varepsilon_a(z)) \tag{8.12}$$

in which the actual strain at level z, $\varepsilon_a(z)$, is given by:

$$\varepsilon_a(z) = (1 - R_N) \cdot \Delta\varepsilon_i + (1 - R_M) \cdot \Delta\phi_i \cdot (z - z_{\text{cen}}) \tag{8.13}$$

where

R_N coefficient defining the degree of the external axial restraint; practical axial restraint factors for common situations may be taken from Fig. 8.8,

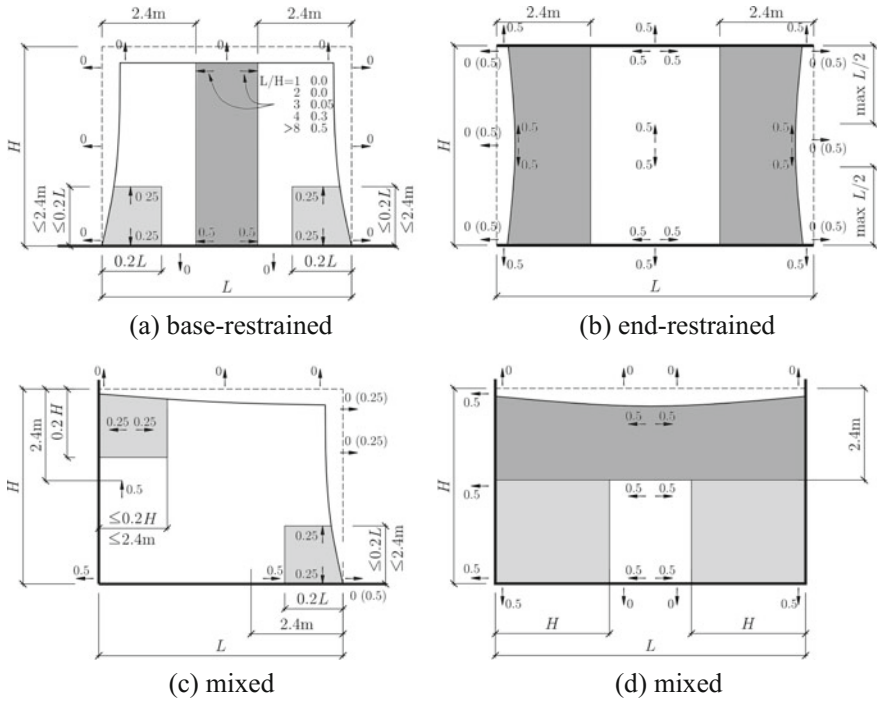

Fig. 8.8 Restraint coefficients in typical situations according to (EN 1992-3 2008)

R_M coefficient defining the degree of the moment restraint (EN 1992-3 2008) states that in a lot of cases the value of $R_M = 1$ can be assumed,
$\varepsilon_a(z)$ actual strain at level z,
$\varepsilon_i(z)$ imposed strain at level z,
$(z - z_{\text{cen}})$ distance to the section centroid, m.

ACI Committee 207 in (ACI 207.2 2007) proposed a simplified approach, allowing for determination of stresses at the centreline of the element, assuming pure translation (no flexure) of the element. The rotational restraint coefficient is assumed as equal to 1. The translational restraint coefficient is defined as a product of the structural shape restraint coefficient, K_R, and the foundation restraint coefficient, K_F:

$$R_N(z) = K_R(z) \cdot K_F \tag{8.14}$$

The tensile stress at any point on the centreline due to a decrease in length, $\bar{\varepsilon}$, can be calculated from the equation:

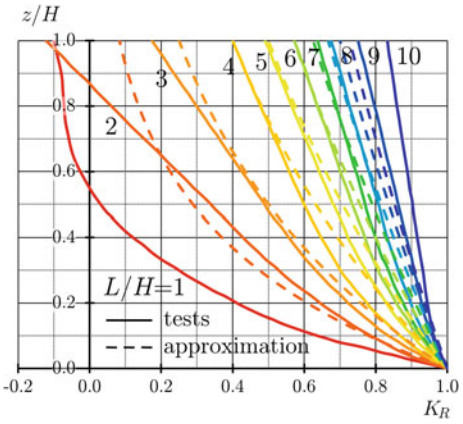

Fig. 8.9 Structural shape restraint coefficient according to (ACI 207.2 2007) after (Knoppik-Wróbel 2015)

$$\sigma(z) = R_N(z) \cdot \overline{\varepsilon} \cdot E_{c,\text{eff}} \tag{8.15}$$

where

$E_{c,\text{eff}}$ effective value of Young's modulus considering creep

The structural shape restraint coefficient, K_R, describes the variation of the restraint with the L/H of the element. The following approximation of K_R distribution is proposed:

$$K_R(z) = \begin{cases} \left[\frac{L/H-2}{L/H+1}\right]^{z/H_W} & \text{for} \quad L/H \geq 2.5 \\ \left[\frac{L/H-1}{L/H+10}\right]^{z/H_W} & \text{for} \quad L/H < 2.5 \end{cases} \tag{8.16}$$

where z signifies the location above the construction joint. The tensile restraint distribution at the centre section is shown in Fig. 8.9.

The restraint stresses decrease in direct proportion to the decrease in stiffness of the restraining foundation material. The foundation restraint coefficient, K_F, was introduced to account for the influence of the foundation stiffness on the restraint of the concrete element:

$$K_F = \frac{1}{1 + \frac{A_W E_W}{A_F E_F}} \tag{8.17}$$

where

$A_W E_W$ axial stiffness of early-age concrete element,

$A_F E_F$ axial stiffness of foundation or other restraining body. For the restraint by the rock, (ACI 207.2 2007) suggests to take $A_F = 2.5A_W$.

(ACI 207.2 2007) elaborates also on the effect of the internal restraint which adds to this of the external restraint. Stress due to the internal restraint is induced by the temperature and moisture difference in cross section and tensile stresses are due to occur at the surface of the element. The value of these stresses can be determined with the equation previously proposed, analogically as for the external restraint, except that the effective restraining plane is the plane of zero stress in the internal stress block (compensation plane). Internal restraint coefficient is introduced; however, no proposal for determination of its value is made.

When the stresses generated at the joint exceed the bond strength, a horizontal crack at the joint is formed and the bond between the two is limited—a slip of the element is observed. This has an influence on further development of stresses in the element. This effect was taken into consideration by Nilsson (2000, 2003). The approach based on CPM introduces a single restraint factor, R, to determine the restraint stress, σ, based on the stress at the total restraint, σ_{fix}:

$$\sigma = R\left(R_0, \delta_{\text{res}}, \delta_{\text{slip}}\right) \cdot \sigma_{\text{fix}} \tag{8.18}$$

with

$$\sigma_{\text{fix}} = E_{c,\text{eff}} \cdot \varepsilon_0 \tag{8.19}$$

where

R_0 plane-section restraint coefficient, which depends on the geometry of the structure as well as the rotational R_{Mz}, R_{My} and translational R_N boundary restraints,

δ_{res} resilience coefficient considering the nonlinear effects,

δ_{slip} slip coefficient which depicts a restraint stresses reduction as a result of slip failure.

The value of δ_{res} changes at the height of the wall and depends on the boundary restraint. It is a product of the basic resilience coefficient and translational and rotational correction coefficients. To simplify, the resilience coefficient is taken as equivalent to the basic resilience coefficient, $\delta_{\text{res}} = \delta_{\text{res}}^0$, and the correction to account for the translational and rotational boundary influence is included by introduction of the effective width of the restraining body, $B_{F,\text{eff}}$, instead of the real width, B_F. The resilience coefficient is analogical to the structural shape restraint factor, K_R, given by (ACI 207.2 2007). The values of δ_{res} are given in diagrams in Fig. 8.10 or can be approximated with a polynomial function:

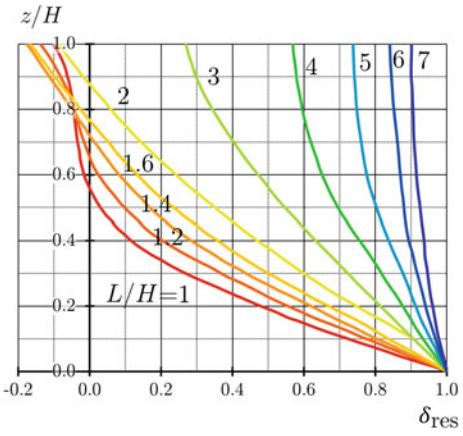

Fig. 8.10 Basic resilience coefficient according to (Nilsson 2000) after (Knoppik-Wróbel 2015)

$$\delta_{\text{res}}^{0} = \sum_{i=1}^{n} a_i \left(\frac{z}{H_W} \right)^i \tag{8.20}$$

where

a_i coefficients of a polynomial function describing resilience coefficient distribution.

The slip coefficient depends on the free length, the width and the height of the casting section. It can be determined experimentally or numerically. The values of δ_{slip} proposed by (Nilsson 2000) are given in diagrams in Fig. 8.11.

The decisive restraint coefficient distribution at height z in the central section of a wall can be calculated according to the following equation:

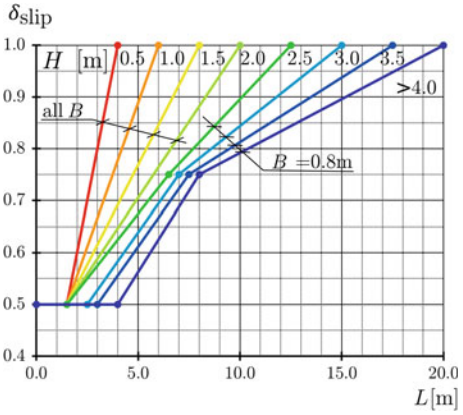

Fig. 8.11 Slip coefficient according to (Nilsson 2000) after (Knoppik-Wróbel 2015)

$$R(z) = \delta_{\text{res}} \cdot \delta_{\text{slip}} - R_0 = \delta_{\text{res}} \cdot \delta_{\text{slip}} - \left(R_N + R_{Mz} + R_{My}\right) \tag{8.21}$$

When the plane-section hypothesis applies, no slip occurs (for the walls with $L/H > 5$), no volume change in the restraining body occurs and there are no translational or rotational boundaries, and the restraint factor can be expressed with an analytic expression (Nilsson 2003):

$$R(z) = 1 - R_0 = 1 - \left(R_N(z) + R_{Mz}(z) + R_{My}(z)\right) \tag{8.22}$$

where R_N, R_{Mz} and R_{My} are given as follows:

$$\begin{aligned}
R_N(z) &= \frac{1}{1 + \frac{E_F}{E_W}\frac{H_F B_{F,\text{eff}}}{H_W B_W}} \\
R_{Mz}(z) &= \frac{(z_{\text{cen}} - z)(z_{\text{cen}} - 0.5H_W)}{\frac{{H_W}^2}{12} + \left(z_{\text{cen}} - \frac{H_W}{2}\right)^2 + \frac{E_F}{E_W}\frac{H_F B_{F,\text{eff}}}{H_W B_W}\left(\frac{{H_F}^2}{12} + \left(z_{\text{cen}} - \frac{H_F}{2}\right)^2\right)} \\
R_{My}(z) &= \frac{\left(y_{\text{cen}} - \omega 0.5\left(B_{F,\text{eff}} - B_W\right)\right)^2}{\frac{{B_W}^2}{12} + \left(y_{\text{cen}} - \omega\frac{B_{F,\text{eff}} - B_W}{2}\right)^2 + \frac{E_F}{E_W}\frac{H_F B_{F,\text{eff}}}{H_W B_W}\left(\frac{{B_{F,\text{eff}}}^2}{12} + {y_{cen}}^2\right)}
\end{aligned} \tag{8.23}$$

When slip failure in the joint is possible and if sections do not remain plane under deformation (high-wall effect), the restraint in the wall is defined as:

$$R(z) = \delta_{\text{slip}} \cdot \left(\delta_{\text{res}}(z) - \left(R_N(z) + R_{Mz}(z) + R_{My}(z)\right)\right) \tag{8.24}$$

where R_N, R_{Mz} and R_{My} are given as follows:

$$\begin{aligned}
R_N(z) &= \frac{\sum_{i=1}^{n}\frac{a_i}{i+1}}{1 + \frac{E_F}{E_W}\frac{H_F B_{F,\text{eff}}}{H_W B_W}} \\
R_{Mz}(z) &= \frac{(z_{\text{cen}} - z)\left(z_{\text{cen}}\sum_{i=1}^{n}\frac{a_i}{i+1} - H_W\sum_{i=1}^{n}\frac{a_i}{i+2}\right)}{\frac{{H_W}^2}{12} + \left(z_{\text{cen}} - \frac{H_W}{2}\right)^2 + \frac{E_F}{E_W}\frac{H_F B_{F,\text{eff}}}{H_W B_W}\left(\frac{{H_F}^2}{12} + \left(z_{\text{cen}} - \frac{H_F}{2}\right)^2\right)} \\
R_{My}(z) &= \frac{\left(y_{\text{cen}} - \omega 0.5\left(B_{F,\text{eff}} - B_W\right)\right)^2}{\frac{{B_W}^2}{12} + \left(y_{\text{cen}} - \omega\frac{B_{F,\text{eff}} - B_W}{2}\right)^2 + \frac{E_F}{E_W}\frac{H_F B_{F,\text{eff}}}{H_W B_W}\left(\frac{{B_{F,\text{eff}}}^2}{12} + {y_{cen}}^2\right)}
\end{aligned} \tag{8.25}$$

The restraint factor can be used as a measure to characterise the stresses induced in the walls; however, the degree of restraint obtained with the numerical and analytic model complies only to some extent. Generally, analytical formulations assume that the degree of restraint increases with an increasing *L/H* ratio. Nevertheless, actually for the same *L/H* ratios, it is not equal but has lower values in walls with larger *L* and *H* dimensions. Also, in case of walls of foundations where the centre of gravity of the combined cross section is located above the wall bottom,

restraint degree can decrease at the bottom. Hence, in determination of the degree of restraint not only the *L/H* ratio but also the individual dimensions of the wall and the restraining body must be taken into account (Knoppik-Wróbel and Klemczak 2015).

8.2.3.2 Simple Prediction of Thermal Stresses in Massive Structures (AIJ 2008)

Recent Japanese guidelines for massive concrete structures: Japanese Concrete Institute (JCI) Guideline (JCI 2008) and Architectural Institute of Japan (AIJ) Guideline (AIJ 2008) suggest that thermal stress analysis in massive concrete structures should be performed with 3D finite element method. The risk of cracking is then assessed with the cracking index (see Sect. 8.2.3.4) where stresses are compared with the actual strength (stress-to-strength ratio). The stress-to-strength ratio (inverse of cracking index) is limited to be less than 0.8 for thermal cracking assessment to avoid the penetration cracks.

The AIJ Guideline proposes also a simple method for prediction of the stress-to-strength ratio for relatively small slab elements (thickness ≤ 3.5 m and length ≤ 40 m) and wall elements (height ≤ 4 m, width ≤ 3.5 m and length 40 m) on the slab with less than 1.0 m thickness. The stress-to-strength ratio can be determined with the charts for a given cement type as shown in Fig. 8.12. According to the slab thickness or wall width and type of cement, the temperature rise (T_{up}) can be estimated (graph I). Then, the cross point between the ratio of the Young's modulus of concrete and soil or rock foundation (E_F/E_c) and length-to-height ratio of the element (L/H_c) in graph II-1 can be extended to the cross point with the foundation's Young's modulus (E_G) in graph II-2. Finally, the point in graph II-2 and the obtained T_{up} are connected to determine the stress-to-strength ratio in graph II-3.

The charts for this graphical method proposed by AIJ Guideline are based on more than 1000 cases and it has been proven that this simple fitting is reasonable for thermal stress cracking risk assessment.

8.2.3.3 An Example of a Simplified Approach

Knowing the evolution of the temperature of concrete, of the Young's modulus, of the relaxation function and of the tensile strength (see Chap. 4), and applying the superposition principle, it is possible to evaluate the stress in case of a uniaxial restrained section from the following equation (see Fig. 8.12):

$$\sigma_t = \sum_{t'=1}^{t' \leq t} CTE \cdot \Delta T(t') \cdot E_c(t') \cdot \psi(t, t') \cdot \gamma_R \tag{8.26}$$

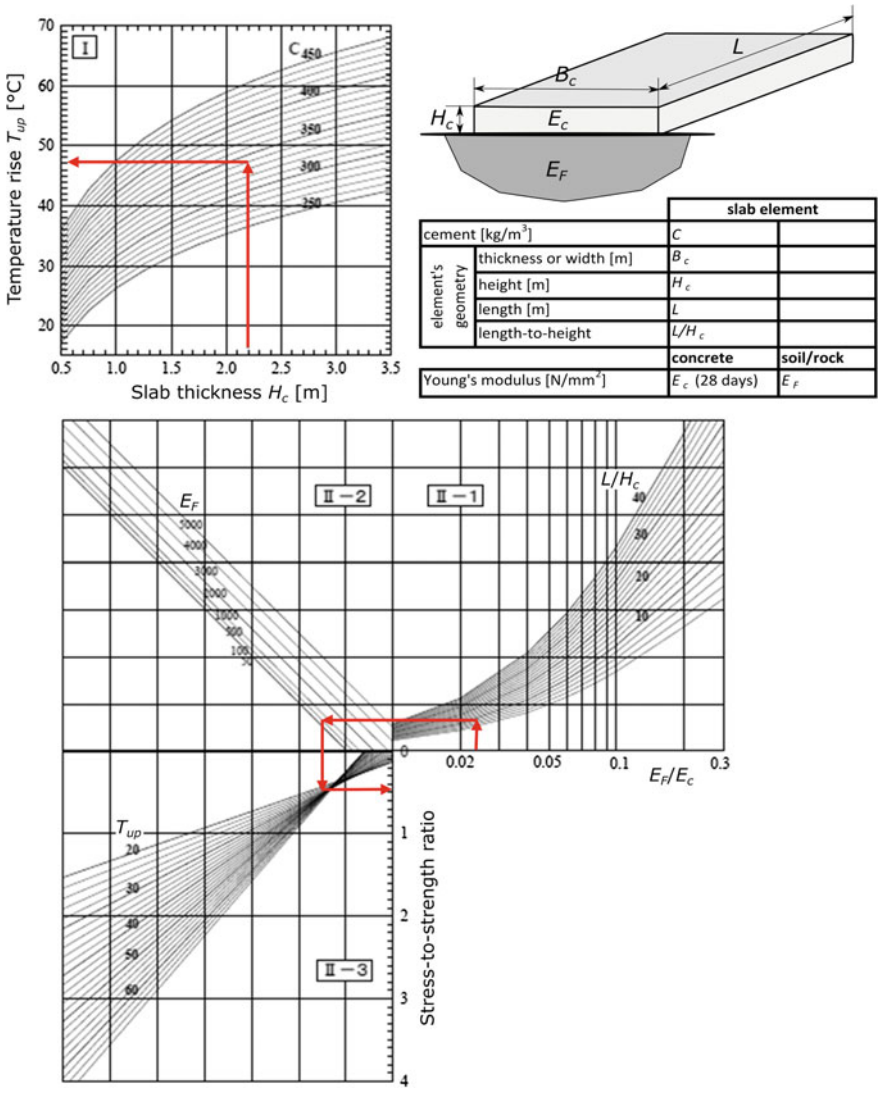

Fig. 8.12 Charts for graphical prediction of stress-to-strength ratio for ordinary portland cement massive concrete structures according to AIJ Guideline (AIJ 2008). Example of red line: C = 340 kg/m^3, H_c = 2.2 m, E_F = 500 N/mm^2, E_c = 24400 N/mm^2, L = 20 m → T_{up} = 47 °C, E_F/E_c = 0.02, stress-to-strength ratio = 0.47

where

t concrete age,
t' the age where load/stress is applied,
$\psi(t,t')$ relaxation function,
γ_R restraint factor (1.0 for fully restrained).

For each time step, these parameters are considered constant.

The variation of concrete stress relaxation function during the first hours after mixing of concrete is very high. Van Breugel (1982) has proposed a relaxation function based on the degree of hydration, which permits to calculate stresses for each incremental increase or decrease of stresses at time t'. The author considered instead of the degree of hydration, due to the complexity in its determination, the Young's modulus of concrete, defining the estimated relaxation that would occur after a time t:

$$\psi(t,t') = \exp - \left[\left(\frac{E_c(t)}{E_c(t')} - 1 \right) + v \cdot t'^{-d} \cdot (t-t')^n \cdot \frac{E_c(t)}{E_c(t')} \right] \tag{8.27}$$

where

v a parameter equal to $0.44w/c$,
d parameter depending on the type of hydration (slow $d = 0.30$, fast $d = 0.40$),
n parameter depending on the type of load (compression $n = 0.30$, tension $n = 0.60$). Equation 8.27 does not consider the effect of autogenous shrinkage and recently the author has proposed to set the n parameter to a single value of 0.30 for both load types.

Figure 8.13 shows examples of the effect of relaxation on the stresses considering different times t_1–t_3 when compared to the elastic evolution (dashed line). The red curve gives the evolution of the stress when all the cumulative stress variations due to relaxation are taken into account.

Figure 8.14 shows an example of the stresses calculated with such an approach till an age of 7 days with a variable daily temperature variation. The red curve

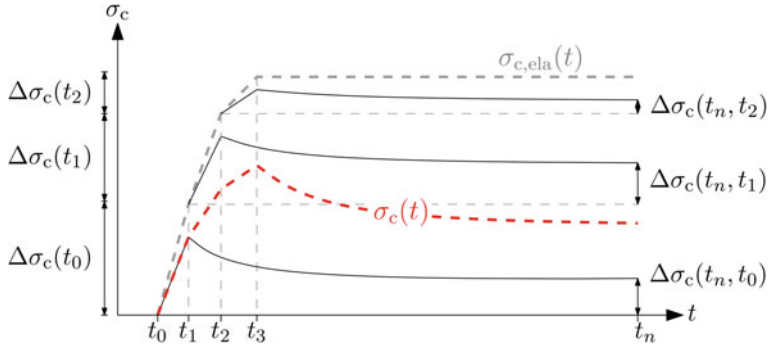

Fig. 8.13 Principle of evaluation of stresses (Schlicke 2014)

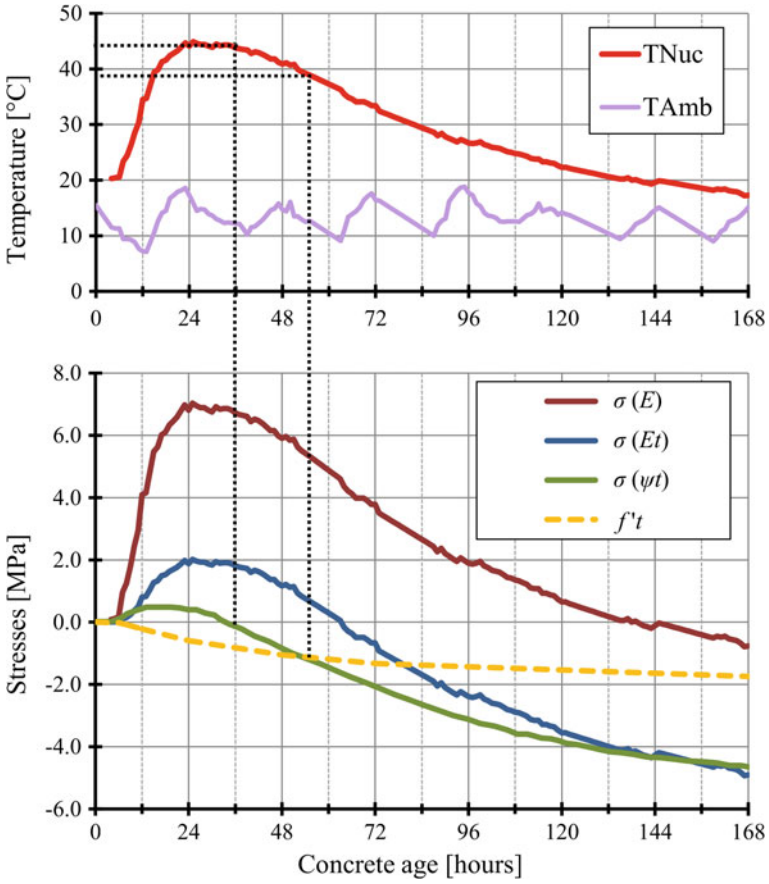

Fig. 8.14 Evolution of measured temperature and calculated stresses with different assumptions. Results by L. Ebensperger (unpublished)

corresponds to the measured concrete core temperature ($T_{max} = 45\,°C$ after 25 h). The green curve is the expected stresses when considering a constant E-modulus for concrete. The blue curve presents the expected stresses when considering an E-modulus for concrete variable in time. And finally, the brown curve is the expected stresses when considering stress relaxation using the incremental equation on a step-by-step calculation. These stresses are compared to the yellow dotted line which corresponds to the expected concrete tensile strength.

Two important temperatures could be noticed:

1. A temperature that corresponds to a stress is equal to zero (second zero temperature). It was reached when concrete showed a temperature of 44 °C after 34 h, just 9 h after reaching the maximal temperature. Each temperature decrease after this moment would generate tensile stresses in the concrete, and the moment of cracking would depend on one hand on how fast the concrete

gains tensile strength, and on the other hand on how fast the concrete loses temperature to the ambient.
2. The moment of the expected occurrence of cracking is achieved after 57 h with a concrete temperature of 38.2 °C, much higher than the ambient temperature.

Note that in case of temperature gradients, additional stresses should be considered and added at the surface level to the stresses that where calculated in this section in order to evaluate the cracking risk.

The theoretical background was gain through different doctoral thesis done at the Baustoffinstitut der TU München (Springenschmid 1987; Breitenbücher 1989; Ebensperger 1990; Schöppel 1993; Mangold 1994) using the 100% restrained cracking frame. The effect of restraint conditions (different than 100%) constant throughout the section may be estimated considering a restraint factor γ_R in Eq. 8.26, and in case of variable restraint conditions in the section, Fig. 8.9 may be used for determination of the tensile stresses. The restraint factor γ_R varies between 0 (free) and 1.0 (fully restrained).

8.2.3.4 Cracking Index

Level I: **Cracking criterion based on average values**

Cracking criteria are used to evaluate the moment of cracking of a hardening concrete element in time. The cracking index is a general description that uses the average values of the actual stress and strength level as a basis for evaluation, running between 0 and 1. A way to use this cracking index, for example proposed in the JSCE guidelines, is to relate the uniaxial tensile stress $\sigma_{ct}(t)$ to the mean concrete tensile splitting strength $f_{ctm}(t)$. In this way, the cracking index changes into:

$$I_{\mathrm{cr}} = \frac{\sigma_{ct}(t)}{f_{ctm}(t)} \tag{8.28}$$

For the mean tensile splitting strength of a normal strength concrete, (Lokhorst 2001; Czerny et al. 2005) developed an experimentally based refined formulation. For this, the ratio between the mean uniaxial tensile strength and the mean tensile splitting strength is explicitly considered with a factor 0.9, yielding into:

$$f_{ctm} = 0.9 \cdot f_{ctm,sp} \tag{8.29}$$

where

f_{ctm} mean uniaxial tensile strength,
$f_{ctm,sp}$ mean concrete tensile splitting strength.

Tensile splitting strength experiments on regular concretes (Lokhorst 2001) have shown cracking index at failure that ranges between 0.75 for a moderate and 0.88

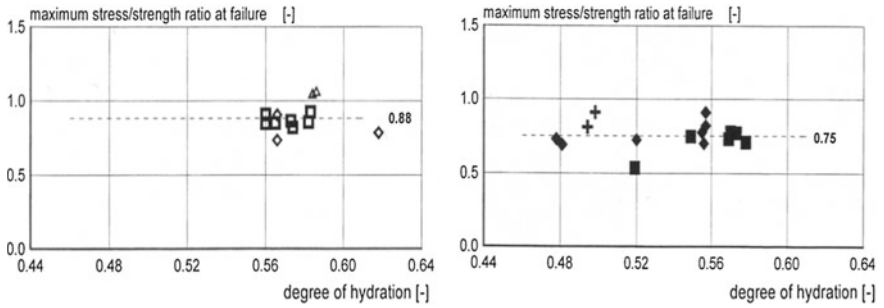

(a) maximum cracking index representing in-situ conditions (restraint deformations)

(b) maximum cracking indexof regular concretes specimens loaded in a laboratory

Fig. 8.15 Maximum cracking index (stress/strength ratio) in different conditions after (Lokhorst 2001)

for a faster loading rate, representing in situ and laboratory conditions, respectively (Fig. 8.15).

Taking this rate effect also into account, representing the difference in loading rates occurring in real-life in situ early-age concretes and rates commonly applied for laboratory testing tensile splitting strength specimens, a value of 0.85 is proposed, leading to the following criterion:

$$\sigma_{ct}(t) \leq 0.9 \cdot f_{ctm,sp,\text{long}} = 0.9 \cdot 0.85 \cdot f_{ctm,sp,\text{short}} \approx 0.75 \cdot f_{ctm,sp} \tag{8.30}$$

where

$f_{ctm,sp,\text{long}}$ mean concrete tensile splitting strength measured at slow loading rates representing loading rates that develop during early-age stress development in hardening concrete structures,

$f_{ctm,sp,\text{short}}$ mean concrete tensile splitting strength measured at high loading rates representing normal laboratory test loading rate conditions.

For high-strength reinforced concrete, (Sule 2003) developed a cracking criterion, where the effect of the materials ductility on the sensitivity towards the rate of loading has been accounted for. Taking this influence into consideration, the following cracking criterion for high-strength concrete was proposed:

$$\sigma_{ct}(t) \leq 0.6 \cdot f_{ctm,sp} \tag{8.31}$$

In the daily construction practise, where the cracking risk has to be defined in the design stage of a project, it is quite common that the tensile stresses should not exceed half of the tensile strength capacity. This general rule is implicitly representing a cracking index of 0.5. Reformulating this design rule for the mean tensile splitting strength leads to the following cracking criterion for the practice:

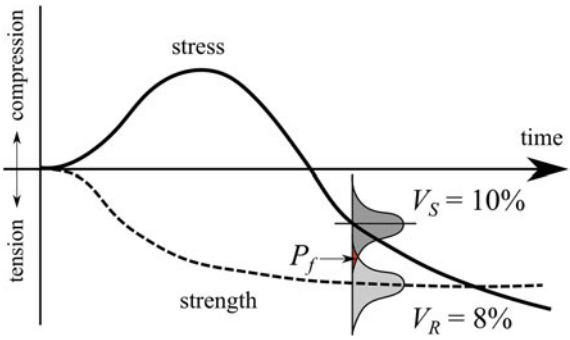

Fig. 8.16 Typical example of mean stress and strength development with time, showing the associated uncertainties expressed in terms of variation coefficients of 10% and 8%, respectively

$$\sigma_{ct}(t) \leq 0.5 \cdot f_{ctm} = 0.45 \cdot f_{ctm,sp} \tag{8.32}$$

In order to take into account the uncertainties on the materials heterogeneity and stress calculations, partial safety factors for both tensile strength and stress have to be applied.

Level II: First-Order Second-Moment Method (FOSM)

Whenever taking into account undetermined influences causing different uncertainties in the actual strength and/or stress level, a more advanced formulation of the cracking criterion is necessary. In this respect, a more detailed probabilistic analysis is required that may follow the Level II approach. Such method is called the first-order second-moment method (FOSM). An indicative example of the tensile stress and tensile strength development over time, in a fresh concrete wall cast on an already hardened floor slab (Fig. 8.6), is provided in Fig. 8.16.

The results also show the uncertainties that go along with both the stress and strength development expressed in terms of statistical variation coefficients with common values of 10% and 8%, respectively. The results show first an increase of the stresses in compression followed by a decrease in tension, following the temperature and autogenous shrinkage developments over time. The strength development follows the properties associated with the mix design.

This so-called first-order second-moment method is a very frequently used method for calculating the cracking risk of hardening massive concrete structures. The method uses the first two statistical moments, i.e. mean value and standard deviation, which represent the stress and strength that develop during a hardening process. When considering the concrete strength to be the resistance R and the stress to be the load S, a general statistical formulation can be derived for the cracking risk, indicated by the overlapping part of the Gauss curves in Fig. 8.16. In this general statistical approach, the uncertainties are assumed to follow a regular Gaussian normal distribution with coefficients of variation for the strength and stress of 10% and 8%, respectively. Cracking occurs whenever the cracking index

has reached a certain critical level, representing equilibrium between the actual tensile strength and tensile stress. Whenever considering the maximum allowable average tensile stress level not to exceed at an average stress level of 75% of the actual mean tensile splitting strength, the probability of failure, representing the event of first crack occurrence, can be defined. After a successful stress and strength computation, the risk of cracking can to be determined from the mean values, σ_S and σ_R, and standard deviations of μ_S and μ_R, respectively. The coefficients of variation are assumed to be $V_S = 10\%$ and $V_R = 10\%$. For the probability of failure, it holds (Koenders et al. 2005, 2007):

$$P_f\{Z = R - S = 0.75 \cdot f_{ctm,sp} - \sigma_{ct} < 0\} = P_f\left\{u < \frac{Z - \mu_Z}{\sigma_Z}\right\} = P_f\left\{u < -\frac{\mu_Z}{\sigma_Z}\right\} \tag{8.33}$$

with

$$\mu_Z = \mu_R - \mu_S \tag{8.34}$$

$$\sigma_Z = \sqrt{\sigma_R^2 + \sigma_S^2} \tag{8.35}$$

where

$$\sigma_R = \mu_R \cdot V_R = \left(0.75 \cdot f_{ctm,sp}\right) \cdot V_R \tag{8.36}$$

and

$$\sigma_S = \sigma_{ct} \cdot V_S \tag{8.37}$$

From this, the risk of cracking of the combined stress-strength system can be calculated from the combined mean value and standard deviation μ_Z and σ_Z, respectively. The cracking uncertainties of the combined system can also be expressed in terms of a so-called safety factor. The safety factor is defined as the ratio between the characteristic strength and the characteristic stress. The characteristic values are determined with a 5% reliability ($\beta = 1.64$). Herewith the safety factor can be calculated, leading to the following equation:

$$\gamma = \frac{R_{\text{char}}}{S_{\text{char}}} = \frac{\mu_R - 1.64 \cdot \sigma_R}{\mu_S + 1.64 \cdot \sigma_S} = \frac{(1 - 1.64 \cdot V_R)}{(1 + 1.64 \cdot V_S)} \cdot \frac{\mu_R}{\mu_S} \tag{8.38}$$

For early-age concrete, R_{char} can be replaced by the characteristic tensile failure strength, which is in this case the tensile splitting strength, and S_{char} by the characteristic stress. Elaboration leads to the following formula for the safety factor:

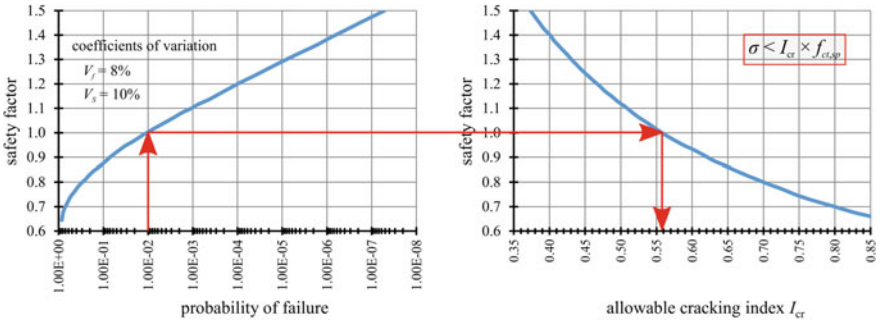

Fig. 8.17 Design graph for determination of the allowable cracking index (stress/strength ratio)

$$\gamma = \frac{f_{\text{char}}}{\sigma_{\text{char}}} = \frac{\left(1 - 1.64 \cdot V_f\right) \cdot 0.75 \cdot f_{ctm,sp}}{\left(1 + 1.64 \cdot V_\sigma\right) \cdot \sigma_{ct}} \tag{8.39}$$

where

V_f variation coefficient of the strength,
V_σ variation coefficient of the stress.

In order to avoid "complex" statistical calculations to calculate the cracking index, a design graph was developed. With this design graph, for a chosen probability of failure a corresponding safety factor and allowable cracking index can be determined that is representing the cracking risk of a massive concrete structure. Or, vice versa, for a calculated cracking index, the corresponding probability of cracking can be obtained. In Fig. 8.17, an example is shown for a probability of failure of $P_f = 10^{-2}$. Via this design graph the related safety factor turns out to be $\gamma = 1.0$ and the maximum allowable cracking index $I_{\text{cr}} = 0.56$. According to the results of this design graph, it is allowed that the cracking index, representing the cracking index, has a maximum value of $I_{\text{cr}} = 0.56$, which is the point where cracking is expected with a probability of occurrence of $P_f = 10^{-2}$. As already mentioned before, in practice, an allowable cracking index of $I_{\text{cr}} = 0.50$ is commonly used for mass concrete structures. This value for I_{cr}, thus, corresponds to a safety factor of $\gamma = 1.12$ and a probability of failure of $P_f = 10^{-3}$.

Level III

A Level III approach is a full probabilistic analysis where the statistical uncertainties of all parameters are taken into account by means of their probability density function, represented by a mean value and standard deviation. Most frequently used calculation method is the so-called Monte Carlo approach, where the variation in the parameters is taken into account by random selection of the parameters from their probability density functions while using this as input data for the analysis. With this calculation procedure, all probability density functions of all

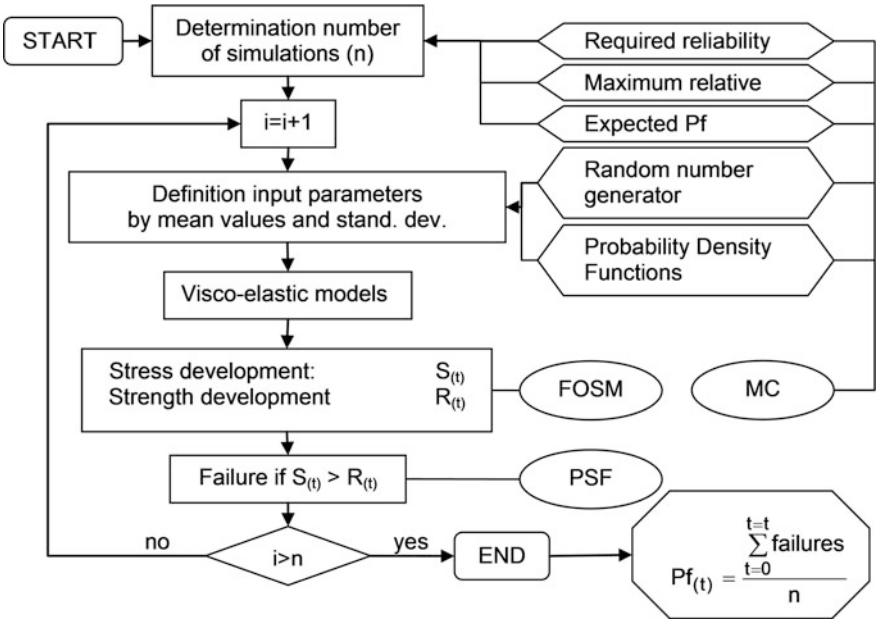

Fig. 8.18 General flowchart of the Monte Carlo approach (MC—Monte Carlo, PSF—partial safety factor and FOSM—first-order second-moment), according to (van der Ham et al. 2006a)

strength and load variables are taken into account. It links the cracking reliability of an element directly to the probability density functions of the stochastic input parameters, which can be either normal or lognormal. Results of laboratory tests or literature data can be used to establish the probability density functions of the input parameters of the early-age cracking problem. This stochastic data can then be used as input for the probabilistic analysis, where different sets of input parameters are generated for each new calculation event, following a Monte Carlo approach. A general flow chart of a Crude Monte Carlo (MC) analysis is shown in Fig. 8.18. The flowchart also indicates the possibility to calculate the level of the partial safety factor (PSF) and the level of the first-order second-moment (FOSM), from the same input data.

The simulation results are used to estimate a probability of failure of a massive concrete system while taking into account all parameter uncertainties. Since all input parameters are considered as random variables, the calculated probability function itself can be treated as a stochastic variable. The uncertainty in the estimation of the system probability will decrease with an increasing total number of simulations (events). For a required system reliability of 95% and a maximum relative error of 0.1, the required number of simulations n should exceed a minimum number of [5, 6]:

Table 8.2 Input data for the Monte Carlo approach, taken from (van der Ham et al. 2006a, b)

Variable	Mean value	CoV [%]	Variable	Mean value	CoV [%]
Material parameters			*External parameters*		
Density—gravel [kg/m^3]	2650	1	Wind speed [m/s]	2	10
Density—sand [kg/m^3]	2650	1	Mean surr. temp [°C]	20	10
Density—cement [kg/m^3]	3150	1	Ampl. surr. temp [°C]	10	20
E_a [kJ/mol]	45.7	10	Initial concrete temp [°C]	20	10
CTE [1/K]	1.2×10^{-5}	5	Construction width [m]	1.00	5
Q_{max} [kJ/kg cement]	440	2.5	Construction height	3.00	2.5
Density—concrete [kg/m^3]	2500	1	Restraint [-]	1.0	10
λ formwork [W/mK]	0.17	10	Formwork thickness [m]	0.02	5
Mix parameters			*Calculation parameters*		
			d age [-]	0.35	10
Air content [%]	1	10	*n* tension [-]	0.30	10
Gravel [kg]	695	10	*n* compression [-]	0.30	10
Sand [kg]	1236	1	E_a—aggregate [MPa]	55000	10
Cement [kg]	350	1	E_p—cement particle [MPa]	55000	10
Water [kg]	150	1	E_c—concrete [MPa]	31000	10

$$n > 400 \cdot \left(\frac{1}{P_f} - 1\right) \tag{8.40}$$

For an arbitrary estimated system probability failure of 0.5, the number of simulations required for this calculation should be at least $n > 400$, which is considered a reasonable number for common analyses on massive concretes.

In Table 8.2, an indicative overview of the most relevant parameters that play a role in the accuracy of the crack risk analysis are presented. In this example, 28 randomly distributed variables are considered, showing their mean value and assumed coefficient of variation (CoV = standard deviation/mean value), and represent their probability density function. All parameters are generated new, following a random likelihood, and used as input for the cracking analysis. This

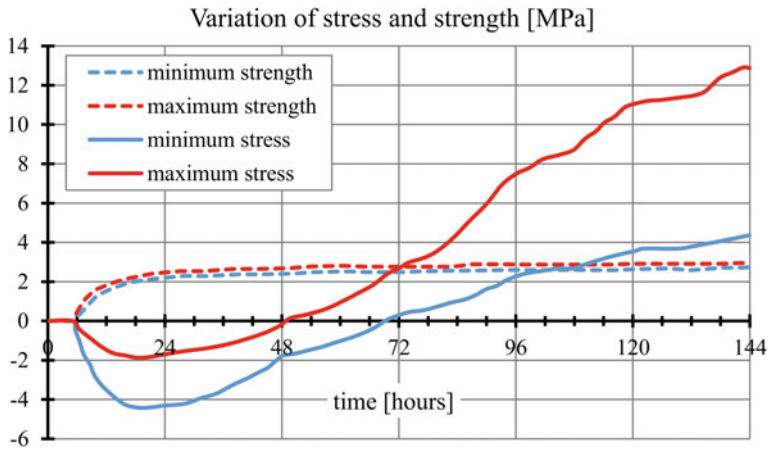

Fig. 8.19 Maximum and minimum stress/strength development from a full probabilistic analysis

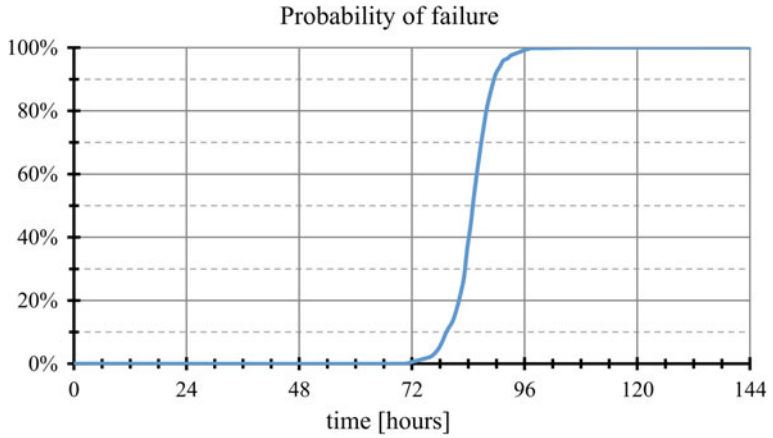

Fig. 8.20 System probability density function calculated with a Level III analysis

procedure will be repeated 400 times and will lead to a system probability function with time calculated from the various stress-strength calculations.

Figure 8.19 shows the results of a regular wall-on-slab structure (Fig. 8.6) assessed according to the Level III full probabilistic analysis. The results show the highest and lowest stress and strength developments with time, being the result of the randomly selected set of input parameters from Table 8.2. From the analysis, it can be seen that the tensile stress exceeds the actual tensile strength somewhere between 72 h (most unfavourable randomly selected parameter combination) and 108 h (most favourable randomly selected parameter combination). These

differences are the result of variations in the input values of the crack risk analysis. Between the 72 and 108 h, the system probability will increase from 0% to 100%, representing a so-called S-curve (see Fig. 8.20). This curve is indicative for all variations in the probabilistic system and shows the pace at which these variation affect the stress-strength development. Whenever comparing this method with the Level I or II methods, it can be observed that those methods consider a probability of failure of 50%, which shows that the Level III method also provides valuable data of the cracking risk already before this value has been reached.

8.2.4 Strain Approach and Strain Capacity

This approach is based on the assumption that cracking is caused by exceeding tensile strain capacity of hardening concrete. The effect of creep and sustained loading is taken into account by introduction of relevant coefficients. CIRIA C660 (Bamforth 2007) is an example of this approach.

The restrained strain due to internal restraint is said to be caused by solely thermal gradient and calculated by introduction of the internal restraint factor:

$$\varepsilon_{\text{int}} = K_1 \cdot CTE \cdot \Delta T \cdot R_i \tag{8.41}$$

where

K_1 coefficient for the effect of stress relaxation due to creep under sustained loading ($K_1 = 0.65$),
ΔT temperature gradient, °C,
R_i internal restraint factor; for the condition of internal restraint, it has been estimated that $R_i = 0.42$.

The restrained strain due to external restraint is calculated by taking into account the long-term thermal and shrinkage deformations as:

$$\varepsilon_{\text{ext}} = K_1 \left[(CTE \cdot T_1 + \varepsilon_{au}) \cdot R_1 + CTE \cdot T_2 \cdot R_2 + \varepsilon_{d,sh} \cdot R_3 \right] \tag{8.42}$$

where

T_1 difference between the peak temperature, $T_{\max}$, and the mean ambient temperature T_a, °C,
T_2 long-term decrease of temperature which takes into account the time of year at which the concrete was cast, °C,
ε_{au} autogenous shrinkage,
$\varepsilon_{d,sh}$ drying shrinkage,
R_1 restraint factor that applies during the early thermal cycle,
R_2, R_3 restraint factors applying to long-term thermal movement and drying shrinkage, respectively.

CIRIA C660 provides a detailed comparison of restraint coefficients in different restraint conditions given by various European standards. It is also commented that the values of restraint coefficient for long-term loads, R_2 and R_3, can be lower than R_1, so application of a single restraint coefficient as proposed by EC2-3 is a conservative approach: assuming that $R_1 = R_2 = R_3 = R$, the maximum value of $K_1 R = 0.5$.

In the strain criterion postulated by CIRIA C660, the expected strain in the hardening element accounting for the restraint, ε/R, is compared with the strain capacity of concrete, ε_{ctu}, calculated as the ratio between the mean tensile strength and the mean Young's modulus, $f_{ctm}(t)/E_{cm}(t)$, which is a lower bound limit value. Nevertheless, given the positive effects of creep on stress and strain relaxation, which can be expressed with a coefficient $K_1 = 0.65$, and sustained loading on tensile properties, which can be expressed with coefficient $K_2 = 0.8$, the actual tensile strain capacity can be increased by $K_2/K_1 = 1.23$.

8.2.5 Simplified Method for Macrocrack Assessment

A simplified method to assess the risk of hardening-induced macrocracks is the comparison of restraint forces with cracking forces. In contrast to the common approach in crack assessment, which is usually based on the overall stresses and failure in material points of a cross section, such procedure concentrates only on the stress resultants in a cross section, whereby the effects of *Eigenstresses* are not pursued. In the context of macrocrack assessment, this simplification is conservative since beneficial influences of the compressive part of *Eigenstresses* were neglected in the uncracked state. At the same time, the tensile part of *Eigenstresses* causes local tensile stress maxima in the cross section; however, *Eigenstresses* begin to disappear to a certain extent as soon as the failure criterion will be reached. The reason is the formation of microcracks or small, locally restricted cracks. Concluding: *Eigenstresses* are beneficial as long as a uncracked state can be presumed—but if cracking cannot be excluded, *Eigenstresses* have only minor importance for the location and width of macrocracks. The underlying model conception is illustrated in Fig. 8.21. For further details, see e.g. (Schlicke and Tue 2015) or (Knoppik-Wróbel and Schlicke 2016).

On basis of these conclusions and with regard to the aimed practicability, the simplified macrocrack assessment is based on an analytical solution. In particular, this will be enabled since only uniformly and linearly in the cross-section distributed deformation impacts need to be considered, whereas nonlinear effects due to temperature and moisture field changes in the cross section can be neglected. Of course, the absolute size of the restraint forces and moments still depends on a complex interaction of thermal and mechanical influences with strict respect to timely variations; however, this can be considered by equivalent temperature impacts with respect to the stiffness of the hardened member. The size of these

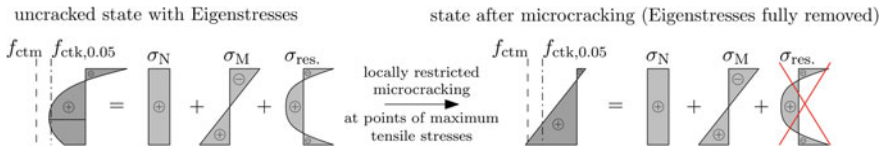

Fig. 8.21 Role of *Eigenstresses* on the process of macrocracking (Schlicke 2014)

equivalent temperature impacts has to be determined beforehand taking into account the hardening behaviour of the concrete as well as thickness of the cross section. But if they are once known, they can easily be provided for practical design, as implemented in related national guidelines of Germany and Austria (BAW 2011; OeBV 2018).

The analytical solution is derived from the equilibrium as well as the deformation compatibility of the present member. The mechanical consistence in such procedure enables both (i) a suitable consideration of the structural response of the member according to the material behaviour and member type and (ii) a realistic consideration of the restraint situation in the individual case. The most common member types affected by the outlined effects are ground slabs and walls on foundations for which the determination of restraint forces and moments is given in the following.

8.2.5.1 Decisive Restraint Forces and Moments in Ground Slabs

The decisive restraint stresses of ground slabs are subject to a superposition of bending restraint and external restraint. In detail, two critical states can be identified: (i) almost pure bending stresses with tension at the top surface at the time of maximum temperature at the bottom surface and (ii) a superposition of bending stresses and centric tensile stresses at the time of temperature equalisation. The according restraint situations are illustrated in Fig. 8.22.

The restraint moment with maximum tension at the top surface occurs shortly after the time of maximum temperature in the interior. At this time, the restraint force is still compression or almost zero and can be neglected. The restraint moment with maximum tension at the bottom surface occurs at temperature equalization. At the same time, the restraint force due to horizontal restraint of the soil is fully developed. Altogether, it holds:

$$M_{F,\text{top}} = -\frac{CTE \cdot \Delta T_{M,\text{eq},F,o}}{h_F} \cdot E_F I_F \leq \frac{\gamma_c \cdot A_F \cdot {L_{F,\text{eff}}}^2}{2} \quad \text{with} \quad N_{F,\text{acc}} = 0 \quad (8.43)$$

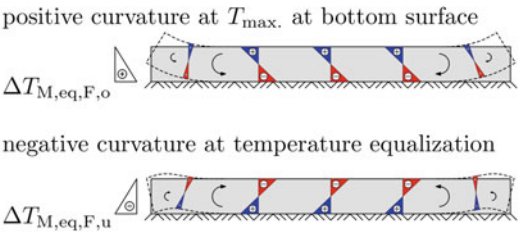

(a) Moments due to temperature gradients

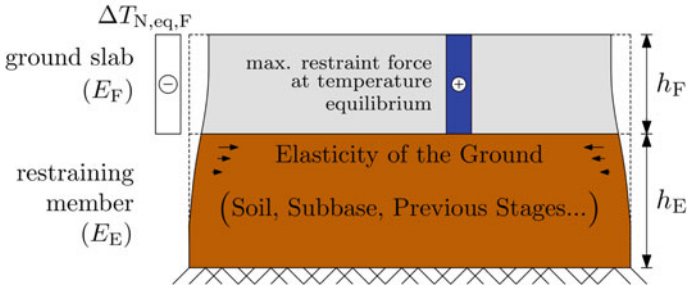

(b) Restraint force due to soil-structure interaction

Fig. 8.22 Equilibrium and stress resultants of ground slabs (Schlicke 2014)

and

$$M_{F,\text{bottom}} = \frac{CTE \cdot \Delta T_{M,\text{eq},F,u}}{h_F} \cdot E_F I_F \leq \frac{\gamma_c \cdot A_F \cdot L_{F,\text{eff}}{}^2}{2} \quad \text{with}$$
$$N_{F,\text{acc}} = -CTE \cdot \Delta T_{N,\text{eq},F} \cdot E_F A_F \cdot R_N \tag{8.44}$$

where

$\Delta T_{M,\text{eq},F,o}$	equivalent temperature gradient in the slab representing a positive curvature (usually at time of maximum temperature at the bottom),
$\Delta T_{M,\text{eq},F,u}$	equivalent temperature gradient in the slab representing a negative curvature (usually at time of temperature equalisation),
$E_F I_F$	bending stiffness of the foundation,
$E_F A_F$	axial stiffness of the foundation,
h_F	thickness of the slab,
γ_c	specific weight of concrete,
$L_{F,\text{eff}}$	distance between free edge of the slab and point of zero deformation,
A_F	cross-sectional area of the ground slab,
R_N	axial restraint degree of ground slab.

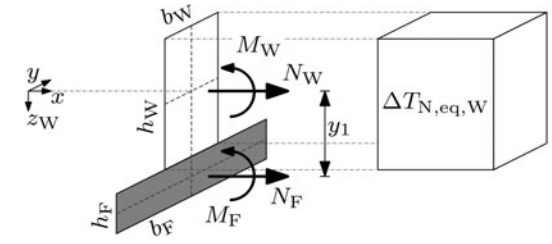

(a) Internal restraint forces

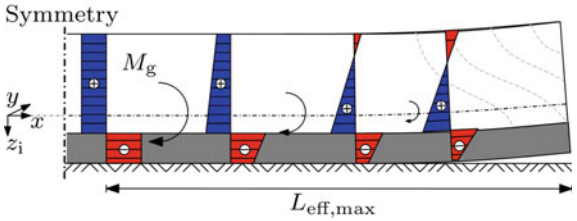

(b) External moment due to self-weight activation

Fig. 8.23 Equilibrium and stress resultants in walls on foundations (Schlicke 2014)

In case of ground slabs, critical stress states may occur on the top surface as well as on the bottom surface. Their size can be determined with:

$$\sigma_{F,\text{top}} = CTE \cdot \frac{\Delta T_{M,\text{eq},F,o}}{2} \cdot E_F \leq 3 \cdot \frac{\gamma_c \cdot {L_{F,\text{eff}}}^2}{h_F}$$

$$\sigma_{F,\text{bottom}} = -CTE \cdot \Delta T_{N,\text{eq},F} \cdot R_N \cdot E_F + \min\left\{ CTE \cdot \frac{-\Delta T_{M,\text{eq},F,u}}{2} \cdot E_F; 3 \cdot \frac{\gamma_c \cdot {L_{F,\text{eff}}}^2}{h_F} \right\} \tag{8.45}$$

8.2.5.2 Decisive Restraint Forces and Moments in Walls on Foundations

The restraint forces and moments of walls restrained by a foundation are subject to the inner deformation compatibility of the cross sections of wall and foundation as well as the activation of self-weight following the curvature of the cross-section compatibility. Figure 8.23 illustrates both with a shortening wall, which is symmetrically located on a foundation.

The internal forces can be determined with:

$$N_W = -CTE \cdot \Delta T_{N,\mathrm{eq},W} \cdot \left(\frac{1}{E_F A_F} + \frac{1}{E_W A_W} + \frac{{y_1}^2}{E_F I_F + E_W I_W} \right)^{-1}$$
$$M_W = N_W \cdot y_1 \cdot \frac{1}{1 + \frac{E_F I_F}{E_W I_W}} \tag{8.46}$$

where

$\Delta T_{N,\mathrm{eq},W}$ equivalent temperature impact in the wall representing the predominant of uniformly in the cross-section-distributed cooling
y_1 inner level arm, usually $(h_W + h_F)/2$.

And the additionally occurring external moment M_g can be determined according to the real member length L by:

$$M_g = \frac{\gamma_c \cdot A_{\mathrm{tot}} \cdot {L_{\mathrm{eff,max}}}^2}{2} \text{ with : } L_{\mathrm{eff,max}} = \sqrt{\frac{2 \cdot M_W}{\gamma_c \cdot A_{\mathrm{tot}}} \cdot \frac{I_i}{I_W}} \leq \frac{L}{2} \tag{8.47}$$

where

A_{tot} area of whole cross section (wall + foundation),
M_W inner moment due to cross-section compatibility,
I_i moment of inertia of whole cross section,
I_W moment of inertia of wall cross section,
L real length of the wall.

The correct consideration of the self-weight activation is of great importance. It is limited to a certain length $L_{\mathrm{eff,max}}$, which depends on geometrical conditions of the cross section as well as the height of the deformation impact. In systems with smaller lengths—which is often the case—there is only a partial activation of the self-weight possible. Finally, the stress distribution without *Eigenstresses* can be determined with:

$$\sigma_{W,\mathrm{bottom/top}} = \frac{N_W}{A_W} + \frac{M_W}{I_W} \cdot z_{W,\mathrm{bottom/top}} + \frac{M_g}{I_i} \cdot z_{i,\mathrm{bottom/top}} \tag{8.48}$$

where

$z_{W,\mathrm{bottom/top}}$ distance between point of gravity in the wall and bottom, respectively, top of the wall,
$z_{i,\mathrm{bottom/top}}$ distance between point of gravity of the whole cross section and bottom, respectively, top of the wall.

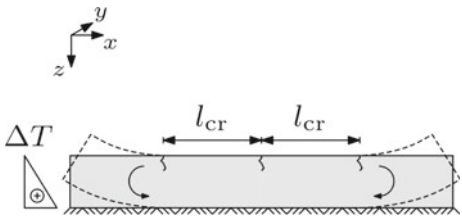

(a) bending cracks due to self-weight activation of a ground slab

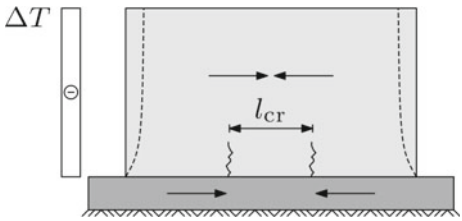

(b) separating cracks due to external restraint of a wall on a foundation

Fig. 8.24 Geometric set crack patterns of typical members which are predominantly restrained (Schlicke 2014)

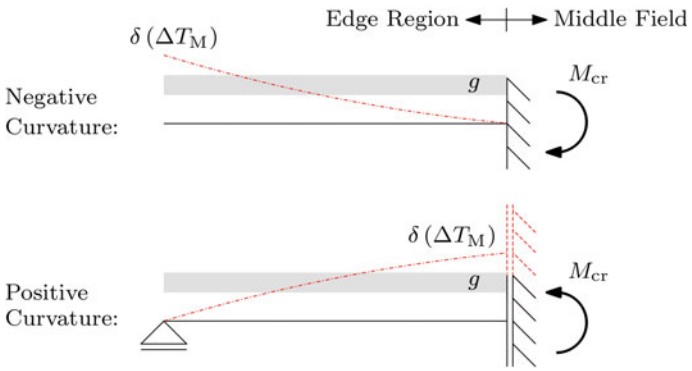

Fig. 8.25 Conceptual model for the distance between primary bending cracks of a ground slab (Schlicke 2014)

8.2.5.3 Crack Risk and Macrocrack Patterns to Be Expected

If the finally determined stresses exceed the present tensile strength $f_{ctm}(t)$, the formation of macrocracks should be assumed. In case of ground slabs, the most likely scenario is bending cracks at the top surface. Pure bending cracks at the bottom surface are almost impossible; however, if the superimpose with additional uniformly over the height distributed stresses according to N_F, the occurrence of

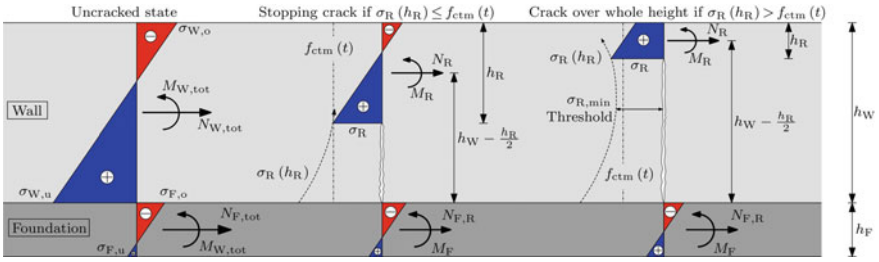

Fig. 8.26 Conceptual model for determination of the crack height in walls restrained by a foundation, based on the stress distribution in the uncracked state (Schlicke 2014)

separating cracks starting from the bottom surface cannot be excluded safely. But this requires unusual high stiffness of the ground in horizontal direction and is thus to be seen as a rare scenario. In case of walls on foundations, the highest stresses occur always at the bottom of the wall and would lead to separating cracks starting from the bottom and proceeding over the height of the wall.

A conservative estimate of the macrocrack pattern to be expected can be derived geometrical considerations, as illustrated in Fig. 8.24. This concentrates only on primary cracks which occur predominantly according to the restraining condition. Additional secondary cracks, which can be created in the surrounding of the primary cracks by activation of reinforcement, were addressed in Sect. 8.4.

In case of ground slabs, the distance between primary cracks predominantly depends on the bending moment according to self-weight activation, whereby the formation of a new crack can be assumed as soon as the cracking moment will be reached. The required length can be estimated using the conceptual model shown in Fig. 8.25.

The length needed to build up the cracking moment holds in both cases:

$$l_{\mathrm{cr}} = \sqrt{\frac{1}{3} \cdot \frac{f_{ctm}(t_{\mathrm{cr}}) \cdot h_F}{\gamma_c}} \tag{8.49}$$

where

$f_{ctm}(t_{cr})$ mean tensile strength of concrete at time of macrocrack formation,
h_F thickness of the slab.

The distance between primary cracks in walls restrained by a foundation is subject to the length needed to build up the axial restraint stresses again. But this length strongly correlates with the height the primary crack reaches. With the assumption of a plane cross section during the whole process of crack formation, the stress redistribution while cracking can be described as illustrated in Fig. 8.26. It should be mentioned that the final restraint force and restraint moment in the wall is to be determined from the results in Eq. 8.48.

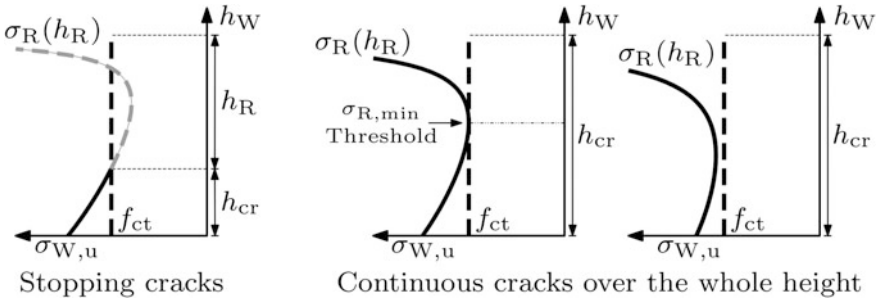

Fig. 8.27 Possible results of the graphically determined crack height in the wall

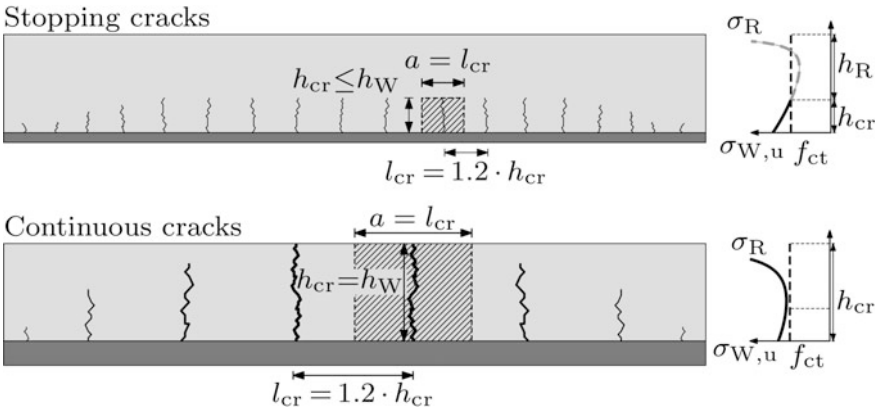

Fig. 8.28 Conceptual model to determine the distance between primary cracks in walls restrained by a foundation depending on the crack height (Schlicke 2014)

The stress at the top of the crack σ_R is of major interest. Its size depends on the remaining concrete height h_R, while the forces of the uncracked state are transferred through the remaining cross section until the crack proceeds over the whole height of the wall. Beginning with crack formation at the wall bottom, σ_R first decreases until a threshold is reached. From this point onwards, the constriction of the concrete area is decisive and σ_R is steadily increasing. Its development can be described with:

$$\sigma_R(h_R) = \frac{\kappa_R \cdot E_W \cdot b_W \cdot \left(h_R{}^3 - h_W{}^3\right) + 6 \cdot N_{W,\text{tot}} \cdot (h_W + h_F)}{6 \cdot b_W \cdot h_R \cdot (2 \cdot h_W - h_R + h_F)} + \frac{\kappa_R \cdot E_W \cdot h_R}{2} \tag{8.50}$$

where

$$\kappa_R = \frac{\sigma_{W,\text{bottom}} - \sigma_{W,\text{top}}}{E_W \cdot h_W} \text{ and } N_{W,\text{tot}} = \left(\sigma_{W,\text{bottom}} - \frac{\sigma_{W,\text{bottom}} - \sigma_{W,\text{top}}}{2}\right) \cdot b_W \cdot h_W$$

If σ_R falls below the tensile strength, the growth of the primary crack can be assumed to stop. The solution of whether or not the growth stops has to be found graphically. Figure 8.27 gives an impression of this approach by introducing the three possible types of solutions, indicating stopping cracks or continuous cracks over the whole height of the wall.

Finally, the distance between the primary cracks in the wall can be estimated according to the illustrations in Fig. 8.28 (Schlicke 2014).

8.3 Crack Width Estimation

To estimate the crack width, the spacing between cracks should be determined. Note that at early age, very often the cracking is not in a stabilised stage. In this case, the length between two cracks is larger and to evaluate the crack width one should use the transfer length over which slip between concrete and steel occurs. Indeed, within this length, steel and concrete strains contribute to the width of the crack. Generally, the equation for the evaluation of the crack width w_k is:

$$w_k = 2 \cdot l_{s,\max} \cdot (\varepsilon_{sm} - \varepsilon_{cm} - \varepsilon_{sh}) \tag{8.51}$$

with

$l_{s,\max}$ transfer length (maximum crack spacing in the stabilised cracking stage),
ε_{sm} mean tensile strain of reinforcement,
ε_{cm} mean tensile strain of concrete,
ε_{sh} shrinkage strain (negative in case of shrinkage).

8.3.1 Model Code 2010

The transfer length is a function of the ratio between $\emptyset$ of the rebars and the reinforcement ratio $\emptyset/\rho_{\text{eff}}$ on one hand and on the concrete cover c on the other hand (Perez Caldentey et al. 2013). The first term can be obtained with a classical bond theory. The second was introduced because of experimental evidences (Beeby 2004). In Model Code 2010, the transfer length is evaluated by means of the following relation:

$$l_{s,\max} = k_2 \frac{\emptyset}{\rho_{\text{eff}}} + k_1 c \tag{8.52}$$

The parameters k_1 and k_2 proposed by Model Code 2010 are fitted on experimental results. The term $(\varepsilon_{sm} - \varepsilon_{cm})$ could be evaluated like in Eurocode 2 (see next section).

8.3.2 Eurocode 2-3

In Eurocode 2 Part 3 (EN 1992-3 2008), two main cases are considered. In the first one, volume changes are restrained along two opposite faces—end-restrained case (Fig. 8.8). In this case, the difference between steel and concrete strains is estimated by the following relation:

$$(\varepsilon_{sm} - \varepsilon_{cm}) = 0.5 \cdot \alpha_e \cdot k_c \cdot k \cdot f_{ct,\text{eff}} \cdot \frac{\left(1 + \frac{1}{\alpha_e \cdot \rho}\right)}{E_s} \tag{8.53}$$

with

α_e the ratio E_s/E_{cm} with E_s the Young modulus of steel and E_{cm} the mean Young modulus of concrete,

k_c and k defined in EN 1992-1-1 as follows: $k = 1$ in the case of webs or flanges, where $h \leq 300\,\text{mm}$, and $k = 0.65$ for webs or flanges where $h > 800\,\text{mm}$, and $k_c = 1$ in direct tension only, $f_{ct,\text{eff}}$ is the mean value of the tensile strength of the concrete effective at the time when the cracks may first be expected to occur,

ρ the ratio between A_s the area of reinforcing steel and A_{ct} the area of concrete within tensile zone just before formation of the first crack.

The second case considers restraint on a base face. In this case, the difference between steel and concrete strains is:

$$(\varepsilon_{sm} - \varepsilon_{cm}) = R_N \cdot \varepsilon_0 \tag{8.54}$$

where

R_N the degree of restraint estimated using methods presented in Sect. 8.2.3.1,

ε_0 the imposed deformation.

8.3.3 ACI 224

In ACI 318 (ACI 318 2014), Chap. 24 Serviceability Requirements, 2014 version, crack control is provided by calculating the probable crack width and proportioning structural elements so that the computed width is less than a predefined value (see Table 8.1). Most equations predict the probable maximum crack width, which usually means that about 90% of the crack widths in the member are below the calculated value.

For one-way slabs (beams), (ACI 224 2001) proposes the following equation to estimate crack width:

$$w = 0.01102 \cdot \beta \cdot f_s \cdot \sqrt[3]{d_c \cdot A} \cdot 10^{-3} \tag{8.55}$$

where

w most probable maximum crack width, mm,
β ratio of distance between neutral axis and tension face to distance between neutral axis and reinforcement steel,
f_s reinforcing steel stress, MPa,
d_c thickness of cover from the extreme tension fibre to the closest bar, mm,
A area of concrete symmetric with reinforcing steel divided by number of bars, mm^2.

8.3.4 JCI Guidelines

In case of JCI Guidelines (JCI 2008), the verification for controlling the crack widths is implemented with the following equation:

$$\gamma_i \frac{w_c}{w_a} \leq 1.0 \tag{8.56}$$

where

γ_i safety factor for verification, generally allowed to be 1.0,
w_a allowable value of crack width,
w_c predicted value of thermal crack width.

The allowable crack width shall be defined based on the application, required performance, surrounding environmental conditions and the concrete cover.

In the guideline, the following equation to predict thermal crack widths is proposed using the thermal cracking index I_{cr}, which was introduced in Sect. 8.2.3.3.

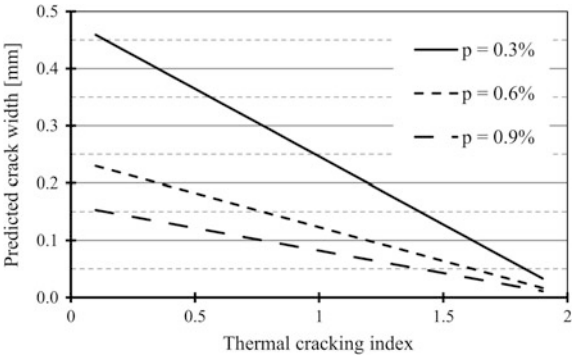

Fig. 8.29 Relation between thermal cracking indices and thermal crack

$$w_c = \gamma_a \left(\frac{-0.071}{\rho} \right) \cdot (I_{\mathrm{cr}} - 2.04) \tag{8.57}$$

$$I_{\mathrm{cr}} = \frac{\sigma(t)}{f_t(t)} \tag{8.58}$$

where

γ_a safety factor to evaluate the thermal crack widths, which shall be 1.0–1.7 depending on the performance requirements,

ρ reinforcement ratio (%, the ratio of the reinforcement area perpendicular the crack direction to the intended concrete area), the applicable range of which is 0.25–0.93%,

$\sigma(t)$ the maximum principal tensile stress at temperature adjusted age of t,

$f_t(t)$ tensile strength at temperature adjusted age of t.

The equation is formulated based on the experimental results of full-size wall specimens subjected to the predominant external restraint at the bottom while assuming insignificant influence of internal restraint and drying. Figure 8.29 gives an example of the relation between thermal cracking indices and thermal crack widths when γ_a is 1.0.

The thermal cracking index is calculated based on thermal and stress analyses, and the thermal crack widths can be derived by Eq. 8.56. Then, it is assessed that the obtained crack widths are less than the allowable crack widths.

The thermal crack index can vary with aging depending on the variation of hydration heat, autogenous shrinkage, restraint conditions and others, but may not be always getting smaller with aging. The thermal crack widths can increase with aging to be convergent gradually. The maximum thermal crack width, however, is not always dependent on the thermal crack index. In the guideline, it is recommended that the maximum thermal crack width obtained by the minimum thermal crack index during the target period can be used to compare with the allowable

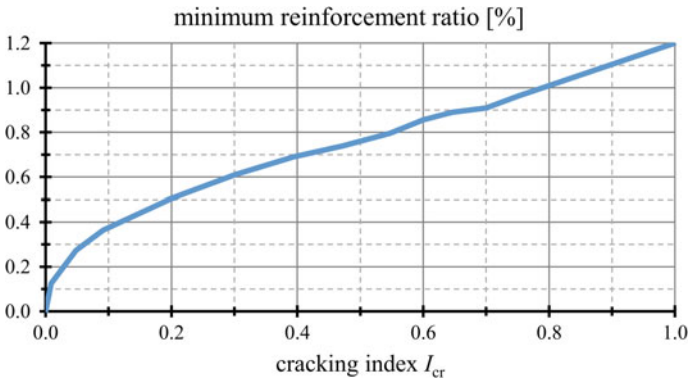

Fig. 8.30 Minimum reinforcement ratios necessary to comply a maximum crack width of 0.2 mm, for various cracking criteria after (van der Ham et al. 2006a)

crack width because it is confirmed that the minimum crack index in the members except the surface and corner is dependent on the maximum crack width.

8.3.5 Return on the Probabilistic Aspects of Cracking

The cracking width that occurs after the tensile stress has exceeded the actual tensile strength may also be considered from a probabilistic point of view. Most advanced method that can link the crack width to the probability of cracking is the Level III method, which is a full probabilistic approach that takes into account all uncertainties of the concrete materials, boundary conditions, geometry, etc., in terms of a probability density function for each individual parameter (see Sect. 8.2.3.4). This so-called stochastic approach considers the cracking risk of hardening concretes from a very detailed and associated uncertainties point of view while considering the influence of uncertainties of all individual parameters into a system probability function that represents all uncertainties in one result. This calculated system probability can also be used to assess the crack width and the most likely crack width, depending on the reinforcement ratio.

Using a method presented before (EN 1992-3 2008 in Sect. 8.3.2 for instance), the crack width can be calculated. For example, for an actual concrete tensile strength of 2.5 MPa and an actual Young's modulus at the moment of cracking of 37 GPa, the reinforcement ratio, needed to control the maximum crack width at 0.20 mm, is 0.97%, when using reinforcement bars of Ø12 mm. Whenever taking the probabilistic aspects into account, uncertainties expressed by the cracking index have to be considered explicitly. As an example, for a representative range of

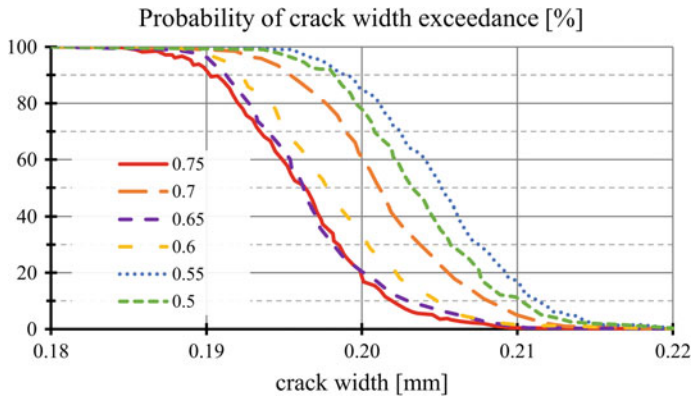

Fig. 8.31 Probability of crack exceedance for different crack criteria after (van der Ham et al. 2006a)

cracking criteria, i.e. ranging from 0.5 to 0.8, the necessary amount of reinforcement has been calculated to comply with the maximum crack width of 0.2 mm. Results are presented in Fig. 8.30, showing the minimum reinforcement versus various cracking criteria. The figure shows a square root type of relationship between the amount of reinforcement necessary and the cracking criterion ($I_{cr} = 0.75 \cdot f_{ctm,sp}/\sigma$), to obey the ultimate crack width of 0.20 mm. In the case of the lower values of I_{cr}, due to the lower tensile strength and Young's modulus at younger ages of the concrete, a relatively higher percentage of reinforcement is needed.

Simulations performed with a Level III calculation result in sets of data, which consist of a cracking time, tensile strength and elastic modulus of the assessed concrete at the moment of cracking, and other relevant data. This information can be used to calculate the crack width for each run. With these crack widths, a probability density function has been constructed, while using various cracking criteria (I_{cr}), i.e. from 0.5 to 0.75, representing probabilities of failure of 10^{-3} and 0.5, respectively (see Fig. 8.17). Results of the probabilities of crack exceedance are provided in Fig. 8.31. The figure shows that for an arbitrary maximum crack width of 0.2 mm, the probability of crack width exceedance is still substantial, and larger cracks are likely to occur in a massive concrete structure. Especially for the lower stress/strength ratios, i.e. 0.5 (cracking index I_{cr}), the probability of larger crack width occurrence is substantial. This shows that in case of critical structures, viz. watertight structures, the cracking criterion in relation to the desired maximum crack width should be considered carefully.

8.4 Reinforcement Design

8.4.1 *Crack Width Control on the Basis of Force Equilibrium*

The characteristically occurring crack width w_k can be derived from the difference of steel strain ε_s and concrete strain ε_c along the crack spacing s_r. By simplifying the real strain distribution along s_r with the introduction of average values, the following correlation can be constituted:

$$w_k = \int_{x=0}^{s_r} (\varepsilon_s - \varepsilon_c)\mathrm{d}x = s_r \cdot (\varepsilon_{sm} - \varepsilon_{cm}) \tag{8.59}$$

In the crack state of single cracks (not all possible cracks have been created along the member length), the difference of steel and concrete strain occurs only in the transfer lengths to both sides of the cracks, whereas stabilised crack patterns (all possible cracks have been created along the member length) are characterised by a difference between steel and concrete strain along the whole member length. On the safe side, the crack spacing can be determined by taking into account the cracking force F_{cr} of the effective concrete area $A_{c,\mathrm{eff}}$ ($F_{\mathrm{cr}} = A_{c,\mathrm{eff}} \cdot f_{ct,\mathrm{eff}}$), the average bond strength and the reinforcement diameter d_s. It holds:

$$s_r = 2 \cdot \frac{F_{\mathrm{cr}}}{\tau_{sm} \cdot \pi \cdot d_s} \tag{8.60}$$

where τ_{sm} is bond stress between reinforcement and concrete.

With respect to the influence of the load duration on the strain distribution in the crack spacing ($k_t = 0.6$ for short term and 0.4 for long term) and the force to be taken by the reinforcement after cracking (F_s), the crack width can be estimated for a given reinforcement (d_s, provided area A_s, elastic modulus E_s) by transformation of Eqs. 8.59 and 8.60 in a form of:

$$w_k = \frac{F_{\mathrm{cr}} \cdot (F_s - k_t \cdot F_{\mathrm{cr}}) \cdot d_s}{2 \cdot \tau_{sm} \cdot E_s \cdot {A_s}^2} \tag{8.61}$$

As long as $F_s \leq F_{\mathrm{cr}}$, only single crack patterns are to be expected and F_s is to set as F_{cr} in Eq. 8.61. If $F_s > F_{\mathrm{cr}}$, all possible cracks will form along the member and a stabilised crack pattern exists. Equation 8.61 considers for both crack states an undisturbed transfer length to both sides of the crack. Strictly seen, this is only correct in case of single cracks. As soon as a stabilised crack pattern has developed, the crack width might be overestimated by Eq. 8.61. The reason is that new cracks may form between neighbouring single cracks so that s_r decreases. Keeping in mind the transition between both crack states and statistical uncertainties of the distance

between cracks in stabilised crack patterns, Eq. 8.61 can be seen as justifiable for both cases. Another crucial point is consideration of the bond stresses between reinforcement and concrete which is usually simplified for conventional reinforcement with an average bond strength along the transfer lengths of $\tau_{sm} = 1.8 \cdot f_{ctm}(t)$. Further details are given in e.g. (König and Tue 2008; König and Tue 1996) or (Tue and Pierson 2001). Finally, the required reinforcement can be determined by transformation of Eq. 8.61 in a form of:

$$A_{s,\mathrm{req}} = \sqrt{\frac{F_{\mathrm{cr}} \cdot (F_s - k_t \cdot F_{\mathrm{cr}}) \cdot d_s}{2 \cdot \tau_{sm} \cdot E_s \cdot w_k}} \tag{8.62}$$

Although several differences can be found in detail, Eqs. 8.61 and 8.62 represent in general the Eurocode 2 regulations for crack width control. The direct determination of the crack width in Eurocode 2 (Sect. 7.3.4) differs only in terms of the empirical determination of the crack spacing, whereas the indirect crack width verification (Sect. 7.3.3, Table 7.2N) can be directly derived from Eq. 8.62. For the relation between crack width, rebar diameter and steel stress can be written according to the same assumptions in Eurocode 2 ($F_s = F_{\mathrm{cr}}$, $k_t = 0.4$, $\tau_{sm} = 1.8 \cdot f_{ctm}(t)$):

$$\sigma_s(w_k) = \sqrt{6 \cdot \frac{w_k \cdot f_{ctm}(t) \cdot E_s}{d_s}} \tag{8.63}$$

The EC2 regulation for the minimum reinforcement (Sect. 7.3.2) bases on the same assumptions and takes up the cracking force respectively the cracking moment. The decisive stress distribution just before cracking is considered by a factor k_c (pure centric restraint $k_c = 1.0$, pure bending restraint $k_c = 0.4$), whereby the absolute size of stresses to be taken up while cracking can be modified empirically for the benefit of an efficient design. These modifications concern positively assumed influences of pre-damage due to residual stresses (factor k) and reduced stresses in case of early-age cracking ($f_{ct,\mathrm{eff}} < f_{ctm}$). Finally, it holds:

$$A_{s,\mathrm{min}} = k_c \cdot k \cdot f_{ct,\mathrm{eff}} \cdot \frac{A_{ct}}{\sigma_s(w_k)} \tag{8.64}$$

The application of Eqs. 8.62–8.64 takes place in the context of a verification of the force equilibrium without further respect to the type of stressing, as outlined in (Schlicke and Tue 2016). While this is very suitable for cases with external loads, such strategy has to be seen critically in cases with significant restraints. The main reason is that the restraint force depends strongly on the deformation compatibility and this includes also its decreasing by formation of any new crack. Furthermore, the crack pattern due to imposed deformations depends predominantly on the

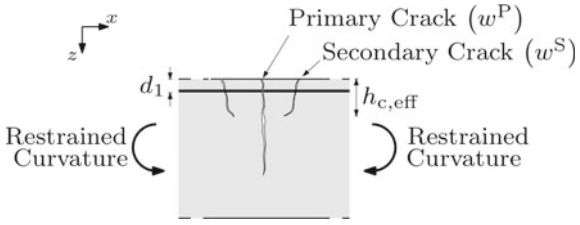

(a) bending cracks
(bending restraint over the thickness)

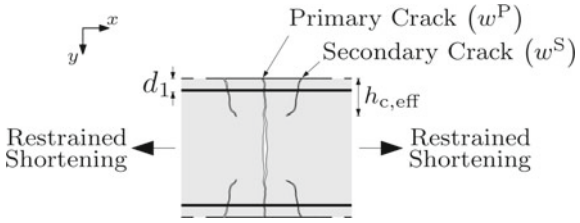

(b) separating cracks
(centric restraint over the thickness)

Fig. 8.32 Crack systems consisting of a primary crack and secondary cracks, here $A_{c,\text{eff}} < A_c$ (Schlicke and Tue 2015)

restraining condition which leads to geometrically set patterns of cracks, as exemplified in Fig. 8.22. Only exception is to systems in which the steel force in the reinforcement is in complete equilibrium with the restraint force, e.g. end-restrained tension rods.

Common reinforcement amounts have no influence on the occurrence of these geometric set crack patterns. Increasing reinforcement degrees would slightly reduce l_{cr}; however, the steel stress in the primary cracks is not affected by the formation of a new primary crack. Thus, these primary cracks can be assumed to be independent from each other, or in other words, the geometric set cracks separate the member in parts with a length of l_{cr} for which crack width control can be carried out independently.

The size of l_{cr} depends predominantly on the member type and restraining situation, whereby two principal cases can be distinguished for practical design. One is the restraining of a curvature due to self-weight activation (e.g. ground slab with temperature gradient over the height), the other one is the interaction with an rigidly connected, restraining component (e.g. shortening of a wall on a foundation). For these typical member types, robust engineering models were presented in Sect. 8.2.5. However, a generally valid model considering the present reinforcement would require further investigations, see (Knoppik-Wróbel and Schlicke 2016).

Besides, it needs to be said that the anchorage of the reinforcement will create secondary cracks next to the primary cracks, as shown in Fig. 8.32 for all cases with significant smaller effective concrete area ($A_{c,\text{eff}} < A_c$).

8.4.2 Crack Width Control on the Basis of Deformation Compatibility

Deformation compatibility is the comparison of deformation impacts in the material with the deformation response of the system. Predominant impacts are thermal expansion ($CTE \cdot \Delta T$), shrinkage due to hydration and drying ($\varepsilon_{au} + \varepsilon_{d,sh}$) as well as creep ($\varepsilon_{cr}$), whereas the system response mainly consists of free deformation ($\Delta l/l$) and restrained deformation in a form of restraint stresses (σ_{rest}/E_c). If the ratio between restraint stresses and real length changes is expressed by a so-called restraint degree R, it can be written in the uncracked state:

$$\left(CTE \cdot \Delta T + \varepsilon_{au} + \varepsilon_{d,sh} + \varepsilon_{cr}\right) \cdot R = -\frac{\sigma_{\text{rest}}}{E_{\text{c}}} \tag{8.65}$$

If restraint stresses exceed a certain limit value of the tensile strength, cracking is to be expected. After cracking, the deformation compatibility has to take into account the cracks with their certain width as well. As explained before, the geometric set cracks separate the member in independent parts with a length of l_{cr}, so that the deformation compatibility can be verified representatively for one primary crack in the length of l_{cr}. Besides, the stiffness of the restrained member decreases due to cracking, so that the restraint degree increases in all cases where the restraining condition is the same after cracking. With regard to the restrained deformation in the transfer length, it can be written for the cracked state:

$$\left(CTE \cdot \Delta T + \varepsilon_{au} + \varepsilon_{d,sh} + \varepsilon_{cc}\right) \cdot R^{\text{II}} \cdot l_{\text{cr}} = -\left[\frac{\sigma_{\text{rest}}^{\text{II}}}{E_{\text{c}}} \cdot \left(l_{\text{cr}} - s_r \cdot (1 - k_t)\right) + w\right] \tag{8.66}$$

and on the basis of the equilibrium between steel force in the primary crack and concrete force in the uncracked part between the primary cracks, the crack width amounts:

$$w = -\left(CTE \cdot \Delta T + \varepsilon_{au} + \varepsilon_{d,sh} + \varepsilon_{cc}\right) \cdot R^{\text{II}} \cdot l_{\text{cr}} - \frac{\sigma_{\text{s}} \cdot A_{\text{s}}}{E_{\text{c}} \cdot A_{\text{c}}} \cdot \left(l_{\text{cr}} - s_r \cdot (1 - k_t)\right) \tag{8.67}$$

Finally, the required reinforcement to limit the crack width under consideration of the deformation compatibility amounts:

$$A_{\text{s}} = \frac{w_{\text{k}} + \left(CTE \cdot \Delta T + \varepsilon_{au} + \varepsilon_{d,sh} + \varepsilon_{cc}\right) \cdot R^{\text{II}} \cdot l_{\text{cr}}}{\left(l_{\text{cr}} - s_r \cdot (1 - k_t)\right)} \cdot \frac{E_c A_c}{\sigma_s(w_k)} \tag{8.68}$$

The solution of Eq. 8.68 is not trivial, and challenging tasks are especially:

- determination of the restraint degree after cracking, in particular if present reinforcement has significant influence,

- consideration of remaining concrete stresses in the uncracked part between two primary cracks, especially if these stresses vary over the height of the cross section and along the member length as in case of bottom-restrained members (e.g. walls on foundations) and
- consideration of secondary cracking.

A possible simplification is that the primary crack, respectively the crack system consisting of primary crack and secondary cracks, will have to absorb the entire restrained deformation of the uncracked state. In practical cases, this assumption is conservative because the restrained deformation in the concrete between primary cracks after cracking is neglected, even though it is bigger than the influence of any possible increase of the restraint degree after cracking. But it is also appropriate because demanding iterations due to the above-listed points can be avoided. It holds:

$$w^P + \sum_{i=1}^{n} w_i^S = \frac{\sigma_{\text{rest}}}{E_{\text{c}}} \cdot l_{\text{cr}} \tag{8.69}$$

The basic idea of Eq. 8.69 is to create as many secondary cracks in the surrounding of the primary crack as needed to limit the crack width in the primary crack. The required number of secondary cracks can be determined with regard to the crack width criteria w_k and the simplification behind Eq. 8.69 by:

$$n = \left(\frac{\sigma_{\text{rest}}}{E_{\text{c}}} \cdot l_{cr} \cdot \frac{1}{w_k} - 1 \right) \cdot 1.1 \tag{8.70}$$

The decreasing width of subsequently occurring secondary cracks in comparison to the width of the primary crack is expressed by the factor 1.1 which covers relevant practical situations.

The minimum reinforcement required can be derived from the number of secondary cracks n, where n is rounded up to the next integer. If $n \leq 0$, the deformation compatibility is already fulfilled with the width of the primary crack and reinforcement for crack width control is not needed. Only a skin reinforcement taking up the cracking force of the effective concrete area would be recommended. All other cases require active crack width control and the required minimum reinforcement can be determined according to Bödefeld (2010). Altogether, it holds:

$$n \leq 0: \quad A_{s,\text{req}} = \frac{f_{ctm}}{f_{yk}} \cdot A_{c,\text{eff}} \tag{8.71}$$

with

f_{ctm} average tensile strength,
f_{yk} yield strength of reinforcement,
$A_{c,\text{eff}}$ effective concrete area (usually $2.5 \cdot d_1 \cdot b$).

$$n > 0: \quad A_{s,\text{req}} = \sqrt{\frac{d_s \cdot b^2 \cdot {d_1}^2 \cdot f_{ctm}(t_{\text{cr}}) \cdot (0.69 + 0.34 \cdot n)}{w_k \cdot E_s}} \tag{8.72}$$

with

d_s	reinforcement diameter,
b	width in direction viewed (normally 1 m),
d_1	edge-distance of the reinforcement,
$f_{ctm}(t_{cr})$	mean tensile strength of concrete at time of macrocrack formation,
n	mean number of required secondary cracks,
w_k	characteristic crack width or crack width criterion,
E_s	Young's modulus of reinforcing steel.

The restraint stresses to be considered in Eqs. 8.69 and 8.70 should represent the maximum stresses due to restraint forces and restraint moments without the effect of *Eigenstresses*. As explained in Sect. 8.2.5, *Eigenstresses* may have a significant influence on the risk of cracking but their effect on the resulting width of macrocracks is negligible.

References

ACI Committee 207. (2005). ACI 207.1R-05: Guide to mass concrete.

ACI Committee 207. (2007). ACI 207.2R-07: Report on thermal and volume change effects on cracking of mass concrete.

ACI Committee 224. (2001). ACI 224R-01: Control of cracking in concrete structures.

ACI Committee 318. (2014). ACI 318–14: Building code requirements for reinforced concrete.

Architectural Institute of Japan. (2008). *Recommendations for practice of thermal cracking control of massive concrete in buildings*. Maruzen Co., Ltd. (in Japanese).

Bamforth, P. B. (2007). *CIRIA C660: Early-age thermal crack control in concrete*. London: CIRIA.

Barre, F., Bisch, P., Chauvel, D., Cortade, J., Coste, J.-F., Dubois, J.-P. et al. (2016). *Control of cracking in reinforced concrete structures: Research project CEOS.fr*. Hoboken, NJ: Wiley.

BAW—German Federal Waterways Engineering and Research Institute. (2011). *BAW Code of Practice: MFZ—Limitation of crack widths resulting from thermal restraint due to hydration heat in solid structural elements*.

Beeby, A. W. (1972). *A study of cracking in reinforced concrete members subjected to pure tension.* Technical report, Cement and Concrete Association, London.

Beeby, A. W. (2004). The influence of the parameter $\emptyset/\rho_{\text{eff}}$. On crack widths. *Structural Concrete*, *5*(2), 71–85.

Bödefeld, J. (2010). *Rissmechanik in dicken Stahlbetonbauteilen bei abfließender Hydratationswärme*. Ph.D. Thesis, University of Leipzig (in German).

Borosnyoi, A., & Snobli, I. (2010). Crack width variation within the concrete cover of reinforced concrete members. *Journal of Hungarian Scientific Society of the Silicate Industry, 3,* 70–74.

Breitenbücher, R. (1989). *Zwangsspannungen und Riβbildung infolge Hydratationswärme*. Ph.D. Thesis, Technical University of Munich (in German).

CEB-FIP *fib*. (2012). Bulletin 65. *Model code 2010: Final draft* (Vol. 1).

Czerny, F., Koenders, E. A. B., & van Breugel, K. (2005). On the reliability of crack predictions for hardening concrete structures. In *Proceedings of 6th International Global Construction Conference, Dundee*.

Ebensperger, L. (1990). *Wirksamkeit von Quellzusätzen im Beton zur Kompensation von Zwangsspannungen infolge Hydratationswärme*. Ph.D. Thesis, Technical University of Munich (in German).

European Concrete Platform. (2008). Eurocode 2 commentary. Brussels.

EN 1992-1-1. (2004). Eurocode 2—Design of concrete structures. Part 1-1: General rules and rules for buildings.

EN 1992-3. (2008). Eurocode 2—Design of concrete structures. Part 3: Liquid retaining and containment structures.

Flaga, K., & Furtak, K. (2009). Problem of thermal and shrinkage cracking in tanks vertical walls and retaining walls near their contact with solid foundation slabs. *Architecture–Civil Engineering–Environment*, *2*(2), 23–30.

Japanese Concrete Institute. (1985). Technical committee report of thermal stress in massive concrete structures (in Japanese).

Japanese Concrete Institute. (2008). Guidelines for control of cracking of mass concrete.

JSCE. (2011). Guidelines for Concrete. No. 15: Standard Specifications for Concrete Structures. Design.

Knoppik-Wróbel, A. (2015). *Analysis of early-age thermal–shrinkage stresses in reinforced concrete walls*. Ph.D. Thesis. Silesian University of Technology, Gliwice, Poland.

Knoppik-Wróbel, A., & Klemczak, B. (2015). Degree of restraint concept in analysis of stresses in early age concrete walls. *Engineering Structures, 102,* 369–386.

Knoppik-Wróbel, A., & Schlicke, D. (2016). Computational prediction of restraint-induced crack patterns in reinforced concrete walls. In *Proceedings of MSSCE2016/Service Life Segment, Lyngby, Denmark* (Vol. 1, pp. 49–58).

Koenders, E. A. B., Czerny, F., & van Breugel, K. (2005). A design concept for crack predictions in hardening concrete structures. In N. Banthia, T. Uomoto, A. Bentur, & S. P. Shah (Eds.), *Proceedings of ConMat '05*, *Vancouver* (pp. 1–10) 2005.

Koenders, E. A. B., van der Ham, H., & van Breugel, K. (2007). Modern statistical methods for accessing the hardening process of concrete. In *Advances in construction materials 2007, part VI* (pp. 471–477).

König, G., & Tue, N. V. (2008). *Grundlagen des Stahlbetonbaus* (3 Auflage). Vieweg + Teubner Verlag (in German).

König, G., & Tue, N. V. (1996). *Grundlagen und Bemessungshilfen für die Rissbreitenbeschränkung im Stahlbeton und Spannbeton*. (DAfStb Heft 466). Berlin: Beuth-Verlag (in German).

Lokhorst, S. J. (2001). *Deformational behavior of concrete influenced by hydration related changes of the microstructures*. Technical University of Delft.

Mangold, M. (1994). *Die Entwicklung von Zwang- und Eigenspannungen im Betonbauteilen während der Hydratation*. Ph.D. Thesis, Technical University of Munich.

Mihashi, H., & Leite, J. P. (2004). State-of-the-art report on control cracking in early age concrete. *Journal of Advanced Concrete Technology, 2*(2), 141–154.

Nilsson, M. (2000). *Thermal cracking of young concrete. Partial coefficients, restraint effects and influence of casting joints*. Licentiate thesis, Luleå University of Technology.

Nilsson, M. (2003). *Restraint factors and partial coefficients for crack risk analyses of early age concrete structures*. Ph.D. Thesis, Luleå University of Technology.

OeBV Österreichische Bautechnik Vereinigung. (2018). Analytisches Bemessungsverfahren für die Weiße Wanne optimiert, Merkblatt (in German).

Pérez Caldentey, A., Corres Peiretti, H., Peset Iribarren, J., & Giraldo Soto, A. (2013). Cracking of RC members revisited: influence of cover, $\emptyset/\rho_{s,ef}$ and stirrup spacing—an experimental and theoretical study. *Structural Concrete*, *14*(1), 69–78.

RILEM TC 119-TCE. (1997). Avoidance of thermal cracking in concrete at early ages. *Materials and Structures*, *30*, 451–464.

RILEM TC 181-EAS. (2002). Early age cracking in cementitious systems—Report of RILEM Technical Committee TC 181-EAS.

Schlicke, D., & Tue, N. V. (2015). Minimum reinforcement for crack width control in restrained concrete members considering the deformation compatibility. *Structural Concrete, 16*(2), 221–232.

Schlicke, D. (2014). *Mindestbewehrung für zwangbeanspruchten Beton*. Ph.D. Thesis, Graz University of Technology (in German).

Schlicke, D., & Tue, N. V. (2016). Crack width control—verification of the deformation compatibility versus covering the cracking force. In *Proceedings of MSSCE2016/Service Life Segment*, Lyngby, Denmark (Vol. 2, pp. 563–572).

Schöppel, K. (1993). *Entwicklung der Zwangsspannungen im Beton während der Hydratation*. Ph.D. Thesis, Technical University of Munich (in German).

Springenschmid, R. (1987). Betontechnologie im Wasserbau. Chapter 1, Wasserbauten aus Beton, Handbuch für Beton-, Stahlbeton- und Spannbetonbau, Hans Blind (in German).

Sule, M. S. (2003). *Effect of reinforcement on early-age cracking in high strength concrete*. Ph.D. Thesis, Delft University of Technology.

Tue, N. V., & Pierson, R. (2001). Ermittlung der Rißbreite und Nachweiskonzept nach DIN 1045. *Beton- und Stahlbetonbau*, *96*, 365–372 (in German).

van Breugel, K. (1982). Development of temperature and properties of concrete as a function of the degree of hydration. In *RILEM International Conference on Concrete at Early Ages*, *Paris* (Vol. 1).

van der Ham, H. W. M., Koenders, E. A. B., & van Breugel, K. (2006a). Level III calculations for hardening concrete elements. In *Proceedings of Integrating Structural Analysis, Risk & Reliability*, *Glasgow* (pp. 1–8).

van der Ham, H. W. M., Koenders, E. A. B., & van Breugel, K. (2006b). Monte Carlo calculations for hardening concrete. In *Proceedings of the European Symposium on Service Life and Serviceability of Concrete Structures ESCS-2006*, *Helsinki* (pp. 189–194).